Charmed Meson Production in 200 GeV/c Pion-Beryllium Interactions

by

Steven S. Sherman

A Thesis
presented to Princeton University
in partial fulfillment of the
requirements for the degree of
Doctor of Philosophy
in
Department of Physics

Princeton, New Jersey

January 1981

I hereby declare that I am the sole author of this thesis.

I authorize Princeton University to lend this thesis to other institutions or individuals for the purpose of scholarly research.

Steven S. Sherman

I further authorize Princeton University to reproduce this thesis by photocopying or by other means, in total or in part, at the request of other institutions or individuals for the purpose of scholarly research.

Steven S. Sherman

ABSTRACT

A THREE ARM SPECTROMETER WITH NARROW ACCEPTANCE AND EXCELLENT PARTICLE IDENTIFICATION WAS USED TO SEARCH FOR CHARGED D* MESON PRODUCTION AT $\sqrt{s}$ = 19.4 GEV. THE SMALL 5.7 MEV Q VALUE FOR THE TWO BODY DECAY D*-> D PI WAS USED AS AN EFFECTIVE BACKGROUND CUT. A 3.0 SIGMA PEAK CONTAINING 82±25 EVENTS IS SEEN IN BOTH THE Q VALUE AND K-PI INVARIANT MASS DISTRIBUTIONS. THIS CORRESPONDS TO $d\sigma/dy|_{y=0}$ = 1.4±.6(STATISTICAL)±.6(SYSTEMATIC) μb/(unit rapidity), WITH ASSUMPTIONS MADE ABOUT THE PRODUCTION MODEL.

ACKNOWLEDGEMENTS

I am greatly indebted to all those who have contributed their resources and talents to Fermilab Experiment 567, the results of which are reported here. The insight and experience of Prof. Val Fitch conceived this experiment and recognized those areas that required close attention as apparatus was constructed, the data accumulated, and the analysis conducted. Prof. Robert Webb designed much of the apparatus and supervised its exacting construction in the short time allotted, while maintaining the cheerful, cooperative atmosphere in which our collaboration worked. Prof. Michael Witherell was resposible for the speedy analysis of the data in this experiment, made possible by his efforts expended in integrating and testing the code used in primary and secondary data analysis. Avram Montag, my fellow graduate student, has fully devoted himself for several years to this experiment.

Our collaborators from Saclay, Torino, and Brookhaven National Laboratory, have supported this experiment with equipment and more importantly, their own technical skill and imagination. My special thanks go to Dr. Brigitte Deveaux for her hard work in integrating the third spectrom-

eter arm, constructed by Saclay, into the rest of the apparatus and computer code.

The High Energy Physics staff at Princeton have given their skill, cooperation, and good humor whole heartedly to this experiment. The data acquisition system designed and constructed by Carl Bopp was simple to use and reliable throughout the experiment, as were the on-line and off-line computer routines written by Victor Bearg. Ann David and Marius Isailia have given knowledgeable advice and aid throughout. The major parts of the detector were designed in detail by Howard Edwards, who also supervised the final mechanical assembly. The detector components built in the Princeton Elementary Particles Laboratory by Walter Bell, Walter Davidson, Nick Diaczenko, Sam Morreale, John Quinn, Richard Rabberman, and William Sands reflected the care taken in its' construction by their ease in assembly and reliability in operation.

This experiment would not have been possible without the cheerful cooperation given by the entire staff at Fermilab, and in particular the Proton area personnel headed by Dr. Ken Stanfield during the data run. Despite the many demands of all the experimenters at the Lab and the limited resources available our requests always were given attention.

Lastly, I would like to thank Professors R. Field and J. Collins for useful conversations concerning QCD, and Professors V. Fitch, R. Webb, M. Witherell, and J. Rosner for their patient and critical reading of this manuscript.

The United States Department of Energy and Veteran's Administration have supported me during this research.

CONTENTS

LIST OF TABLES

LIST OF FIGURES

Chapter I

INTRODUCTION

Since the discovery of the neutron as a fundamental constituent of matter in addition to the proton and electron, determining the spectrum of subatomic particles and a minimal set of descriptive properties for them has been a major direction for physics research. One of the first particle properties described was that of isotopic spin. It was formulated from studies of energy levels in various nuclei and the discovery of the charged and neutral pions. The strong nuclear binding force appeared to be equal for particles within the same group multiplet , so isospin was determined to be a global (space-time independent) symmetry that could be represented by the SU(2) group in the same manner as a particle's intrinsic angular momentum . A rotation in isospin space would transform a proton into a neutron but not affect the part of the mass Hamiltonian that was generated by the strong nuclear force, just as rotations in configuration space leave invariant spin independent Hamiltonian terms.

As particles heavier than the nucleon were discovered during the 1950's a new class appeared that had a lifetime

much greater than could be expected from the energy available for their decay. The characteristic decay signature of long-lived neutral particles caused them to be named "Vee" particles, and it became apparent that a new selection rule inhibited their decay via the strong interaction. It was eventually seen that they could be placed in a SU(3) group spectrum with the previously known particles that belonged to the SU(2) isospin multiplets. The new conserved quantum number leading to the selection rule for decay of particles that interacted with the strong nuclear force was designated "strangeness" and was seen to be conserved by the strong force but not the electromagnetic or weak decay forces.

The SU(3) group has two diagonal generators, corresponding to the observables strangeness and isospin, and three elements in its fundamental irreducible representation. Gell-Mann and Ne'eman formulated the original SU(3) group theory of hadronic phenomena, and Zweig and Gell-Mann independently saw that the group generators could be viewed as building blocks for the hadrons. Gell-Mann named them quarks and assigned them fractional charge and baryon number (1). A theory was developed which used the three different quarks as the fundamental hadronic constituents that successfully predicted magnetic moment ratios and baryon mass differences. The most celebrated success of the SU(3)

theory was Gell-Mann's forecast of a new massive hadron with strangeness = -3, the omega minus, to complete the decuplet of spin 3/2 baryons. All the hadrons discovered before 1974 could be fit into an SU(3) multiplet, either an octet or singlet of quark - antiquark combinations for the mesons or a singlet, octet, or decuplet obtained from coupling together three quarks. Numerous searches for fractionally charged particles were unsuccessful, so the view of quarks as infinite mass mathematical constructs without a physical existence was prevalent for the rest of the decade.

By 1970 analysis of the data from deep inelastic scattering experiments using the 20 GeV/c electron beam at SLAC showed phenomena that was consistent with the existence of point-like , fractionally charged particles within the nucleons. The identification of these particles , dubbed "partons" by Feynman, as quarks was natural. During the next five years various advances in theory gave a sound basis for this identification.

Quite aside from the developments in the understanding of the strong interactions, in 1967 Weinberg and Salam proposed a gauge invariance theory combining the electromagnetic and weak nuclear force. The weak interactions of hadrons could be readily described by the interactions of their constituent quarks. t'Hooft proved that their SU(2) xU(1) local

(space-time dependent) group theory was renormalizable and hence a valid field theory, with the possibility of making predictions based on perturbative calculations. Within two years there was confirmation from a new generation of neutrino experiments of the weak neutral interaction that was a major prediction of the Weinberg-Salam theory.

The success of a field theory with minimally coupled gauge bosons preserving local gauge invariance led to a similar theory for quarks - Quantum Chromodynamics. The non-observation of free quarks could be naturally explained by a force that increased with quark separation, as shown by Politzer and Gross and Wilczek in 1973 (2). Quarks were given a new internal quantum number - color - in addition to the previous quantum numbers of the earlier SU(3) global group theory: strangeness, isospin, electromagnetic charge, and baryon number. The local symmetry leaving the QCD Lagrangian invariant under rotations in color space and satisfying the requirement of asymptotic freedom for the observed number of quark flavors turned out to be SU(3) also. The eight independent generators of SU(3) implied the existence of eight new massless bosons, soon called gluons, that coupled to the color charge on the quarks and other gluons.

Color was not a new concept; Greenberg had postulated in 1964 that quarks obeyed a parastatistics that allowed the existence of an S wave state with J=3/2 and still maintained Fermi statistics for the identical, spin 1/2 quarks (3). Introducing parastatistics was not necessary; it was equivalent to giving the quarks a new hidden quantum number with three eigenvalues. More direct experimental evidence for the existence of three new charges red, blue, and yellow could be found in the measurement of the neutral pion lifetime and R, the ratio of hadronic cross section to the cross section for production of muons in e^+e^- collisions. The lifetime is proportional to the square of the number of colors, while R is equal to the sum of the charges squared of all quarks produced in the e^+e^- collision. Factors of nine and three respectively were needed to reconcile theoretical predictions with measurements of these quantities, showing that each flavor of quark did indeed come in three varieties.

While this new concept of a color charge was verified by experiment, the older global SU(3) theory was running into another trouble area. The rates predicted by SU(3) for the decays $K_L^0 \to \mu^+\mu^-$ and $K^+ \to \pi^+\nu\bar{\nu}$ were much higher than several measurements allowed. This led Glashow, Iliopoulos, and Maiani in 1970 to show how the existence of a fourth quark flavor could eliminate any possibility of low order weak

interaction diagrams causing these decays (4). The existence of a fourth type of quark had been conjectured soon after Gell-Mann's 1963 work by Tarjanne and Teplitz (5) to explain some features of the vector meson spectrum, and by Bjorken and Glashow (6) in a discussion of hadronic weak decay modes and the vector meson system. The two papers called the associated conserved quantum number for this quark supercharge and charm respectively. Amati et al. gave predictions for the new particles and their masses that could be expected in the SU(4) multiplets soon after the Tarjanne and Teplitz paper, and also observed that these "peculiar" particles would be produced in pairs in strong interactions , singly in weak ones, and decay only weakly (7).

The authors of the 1970 paper saw a natural model for suppressing the unobserved weak decay modes in Gell-Mann's 1960 work on weak leptonic currents. By defining a four component vector composed of the known lepton spinors, $\psi = (e, \mu, \nu_e, \nu_\mu)$, the interaction Lagrangian with a Fermi current-current form of weak interaction for leptons may be written as

$$= -ie\bar{\psi}\frac{(1+\tau^3)}{2}\gamma^\mu\psi A_\mu - G_F/\sqrt{2}\,[[\bar{\psi}\gamma_\mu(1+\gamma^5)\frac{\tau^+}{2}\psi][\bar{\psi}\gamma_\mu(1+\gamma^5)\frac{\tau^-}{2}\psi] + \text{h.c.}]$$

where the τ^i are four by four representations of the SU(2) group;

$$\tau^3 = \begin{vmatrix} 1 & 0 & 0 & 0 \\ 0 & 1 & 0 & 0 \\ 0 & 0 & -1 & 0 \\ 0 & 0 & 0 & -1 \end{vmatrix} \quad \tau^+ = \begin{vmatrix} 0 & 0 & 1 & 0 \\ 0 & 0 & 0 & 1 \\ 0 & 0 & 0 & 0 \\ 0 & 0 & 0 & 0 \end{vmatrix} \quad \tau^- = \begin{vmatrix} 0 & 0 & 0 & 0 \\ 0 & 0 & 0 & 0 \\ 1 & 0 & 0 & 0 \\ 0 & 1 & 0 & 0 \end{vmatrix} .$$

Note that this Lagrangian contains no first order neutral couplings proportional to $J^0_L J^0_{L'}$, nor are there any couplings of a J^0_L to a neutral boson field since heavy neutral weak bosons were not postulated until the Weinberg-- Salam theory of 1967. Any induced neutral currents from $J^0 = \frac{i}{2}[J^+, J^-]$ will not contribute to a lepton number changing process because the τ^3 generator is diagonal. Hadronic weak decay phenomena had been well explained by the conserved vector isospin hypothesis and Cabibbo's later extension from conserved currents with SU(2) generators τ^i to vector currents with the SU(3) generators λ^i instead. Weak hadronic currents were of the form:

$$J^{+\mu}_H = i[\bar{\psi}(\tfrac{\lambda^1 + i\lambda^2}{2})\gamma^\mu(1+\gamma^5)\psi]\cos\theta + i[\bar{\psi}(\tfrac{\lambda^4 + i\lambda^5}{2})\gamma^\mu(1+\gamma^5)\psi]\sin\theta$$

where θ is the experimentally determined Cabibbo mixing angle. The SU(3) "charges" associated with these currents are not conserved, but they do obey equal time commutation relations:

$$Q^i = \int \psi^+ \tfrac{\lambda^i}{2} \psi d\mathbf{r} \ , \quad Q^{i5} = \int \psi^+ \tfrac{\lambda^i}{2} \gamma^5 \psi d\mathbf{r}, \qquad [Q_i \ , Q_j] = i f_{ijk} Q^k$$

$$[Q^5_i \ , Q^5_j] = i f_{ijk} Q^k \ , \quad [Q^5_i \ , Q_j] = i f_{ijk} Q^{k5}$$

where the f_{ijk} are the SU(3) structure constants (8).
Using Gell-Mann's choices for the λ^i and defining a three component wave function $\psi = (u \ , d \ , s)$ with the three quark

spinors one gets:

$$J_\mu^{+} = \bar{\psi}\gamma_\mu \begin{vmatrix} 0 & \cos\theta & \sin\theta \\ 0 & 0 & 0 \\ 0 & 0 & 0 \end{vmatrix} (1+\gamma^5)\psi \quad , J_\mu^{-} = \bar{\psi}\gamma_\mu \begin{vmatrix} 0 & 0 & 0 \\ \cos\theta & 0 & 0 \\ \sin\theta & 0 & 0 \end{vmatrix} (1+\gamma^5)\psi$$

$$\text{and,} \quad J_\mu^{0} = \frac{i}{2}[J^+, J^-] = i\bar{\psi}\gamma_\mu \begin{vmatrix} 1 & 0 & 0 \\ 0 & -\cos^2\theta & -\cos\theta\sin\theta \\ 0 & -\cos\theta\sin\theta & -\sin^2\theta \end{vmatrix} (1+\gamma^5)\psi .$$

The off-diagonal elements in the induced hadronic neutral current clearly couple the d and s quarks together to form strangeness changing neutral currents, either current-current couplings with the neutral leptonic weak current or minimal couplings with any neutral weak gauge bosons.

By adding a fourth quark, $\psi \rightarrow \psi = (c, u, s, d)$ and using the same matrices in the current definitions as in the leptonic current but with the unit matrices rotated through the Cabibbo angle the SU(2) current generators:

$$\tau^+ = \begin{vmatrix} 0 & 0 & \cos\theta & -\sin\theta \\ 0 & 0 & \sin\theta & \cos\theta \\ 0 & 0 & 0 & 0 \\ 0 & 0 & 0 & 0 \end{vmatrix} \qquad \tau^- = \begin{vmatrix} 0 & 0 & 0 & 0 \\ 0 & 0 & 0 & 0 \\ \cos\theta & \sin\theta & 0 & 0 \\ -\sin\theta & \cos\theta & 0 & 0 \end{vmatrix}$$

$$\tau^3 = \begin{vmatrix} \cos^2\theta+\sin^2\theta & 0 & 0 & 0 \\ 0 & \cos^2\theta+\sin^2\theta & 0 & 0 \\ 0 & 0 & -\sin^2\theta-\cos^2\theta & 0 \\ 0 & 0 & 0 & -\sin^2\theta-\cos^2\theta \end{vmatrix}$$

are obtained. The induced neutral current J_μ^0 no longer has any off-diagonal elements that can lead to strangeness changing neutral currents and a weak decay for the K_L^0 meson. Electromagnetic decays are still possible and lead to a measured $\Gamma(K_L^0 \rightarrow \mu^+\mu^-)/\Gamma(K_L^0 \rightarrow \text{all}) = 8.1\times10^{-9}$ (9).

The new charmed quark allowed the quark fields to be grouped in two left- handed doublets: $\begin{pmatrix} u \\ d_\omega \end{pmatrix}_L$ $\begin{pmatrix} c \\ s_\omega \end{pmatrix}_L$ matching the leptonic doublets: $\begin{pmatrix} e^- \\ \nu_e \end{pmatrix}_L$ $\begin{pmatrix} \mu^- \\ \nu_\mu \end{pmatrix}_L$ giving quarks and leptons an equal footing in the SU(2)XU(1) gauge theory. Maki saw this possibility of a correspondence between lepton and hadron fields in 1963 when proposing a fourth variety of hadronic field (10). The GIM paper pointed out the difficulties in detecting the new class of "charmed" particles because of the large number of hadronic decay modes from heavy non-charmed particles that would swamp any charm signature. They suggested looking in the cleaner environment of neutrino beams or in the e+e- storage rings for the leptonic decay of a new vector meson.

Measurements taken in 1972 when the Cambridge Electron Accelerator was briefly converted into a storage ring seemed to show a rise in the hadron to muon ratio R at c.m. energies greater than 3 GeV, indicating that a threshold for producing a new variety of hadron had been passed, but there was no identification of the new hadron at that time and the CEA program ended shortly afterward. Other attempts to see charm at existing fixed target facilities and new colliding beams at the CERN ISR and SLAC's SPEAR were unsuccessful until the end of 1974 when a group at SPEAR (11) and a group at the Brookhaven AGS (12) simultaneously announced the sighting of a narrow resonance at 3.1 GeV/c^2 interpreted as

a meson consisting of a charmed and anti-charmed quark. Interestingly, the two groups were looking at nearly reversed processes: the Brookhaven experiment looked for e^+e^- pairs produced in hadronic interaction while the SPEAR group was measuring hadron production from e^+e^- interactions. Direct production of the resonance in e^+e^- annhilation indicated the J^{PC} of the new particle was most likely 1^{--}; this was later confirmed by measurements of the interference of the J/ψ resonance production amplitude with the background QED amplitude for $e^+e^- \rightarrow e^+e^-$. The narrowness of the J/ψ resonance, less than 70 KeV, explained the failure of previous searches which had inadequate resolution to identify the narrow resonance structure. It turned out that the J/ψ was about 600 MeV/c^2 too light to decay into states containing bare charmed particles, and the Zweig quark line rule emphatically suppressed any other charm conserving strong decays.

Because of the low background and the ability to tune the two beams to a resonance energy the e^+e^- colliding beam machines at SPEAR and DORIS became ideal locations for studying the properties of the newly discovered class of particles. Various radial excitations of the J/ψ were quickly discovered. Since the mass of the charmed quark was assumed to be much greater than the binding energy of a $c\bar{c}$ system the ψ family of particles was regarded as an ideal system

for testing QCD theory, playing much the same role as the hydrogen spectrum did for QED.

Concurrently the large neutrino detectors starting to operate at CERN and Fermilab began detecting neutrino induced events with two oppositely charged leptons in the final state (13). The kinematics of these events favored charm production by the reactions : $\nu_\mu + d \rightarrow \mu^- + c \rightarrow s + \mu^+ + \nu_\mu$, $\nu_\mu + s \rightarrow \mu^- + c \rightarrow s + \mu^+ + \nu_\mu$, and $\bar{\nu}_\mu + s \rightarrow \mu^- + c \rightarrow \bar{\nu}_\mu + s + \mu^+$ as the source of these leptons (14). Charm production in neutrino beams became a way of exploring the strange quark "sea" of virtual quark pairs.

Extension from SU(3) to SU(4) global symmetry implied that the multiplet families of particles would also be enlarged. As shown in Fig. 1 the two dimensional weight diagram for the lowest mass meson octet expands into a three dimensional 15-plet when a fourth quark is added. Gaillard, Lee, and Rosner laid out the entire set of new particle spectra that could be expected with a fourth heavy quark, along with predictions for important decay modes and other properties in a review of the charm concept written just weeks before the announcement of the J/ψ discovery (15). The search began for new particles with $C \neq 0$.

Figure 1

SU(4) PSEUDO-SCALER MESON 15-PLET QUARK CONTENT

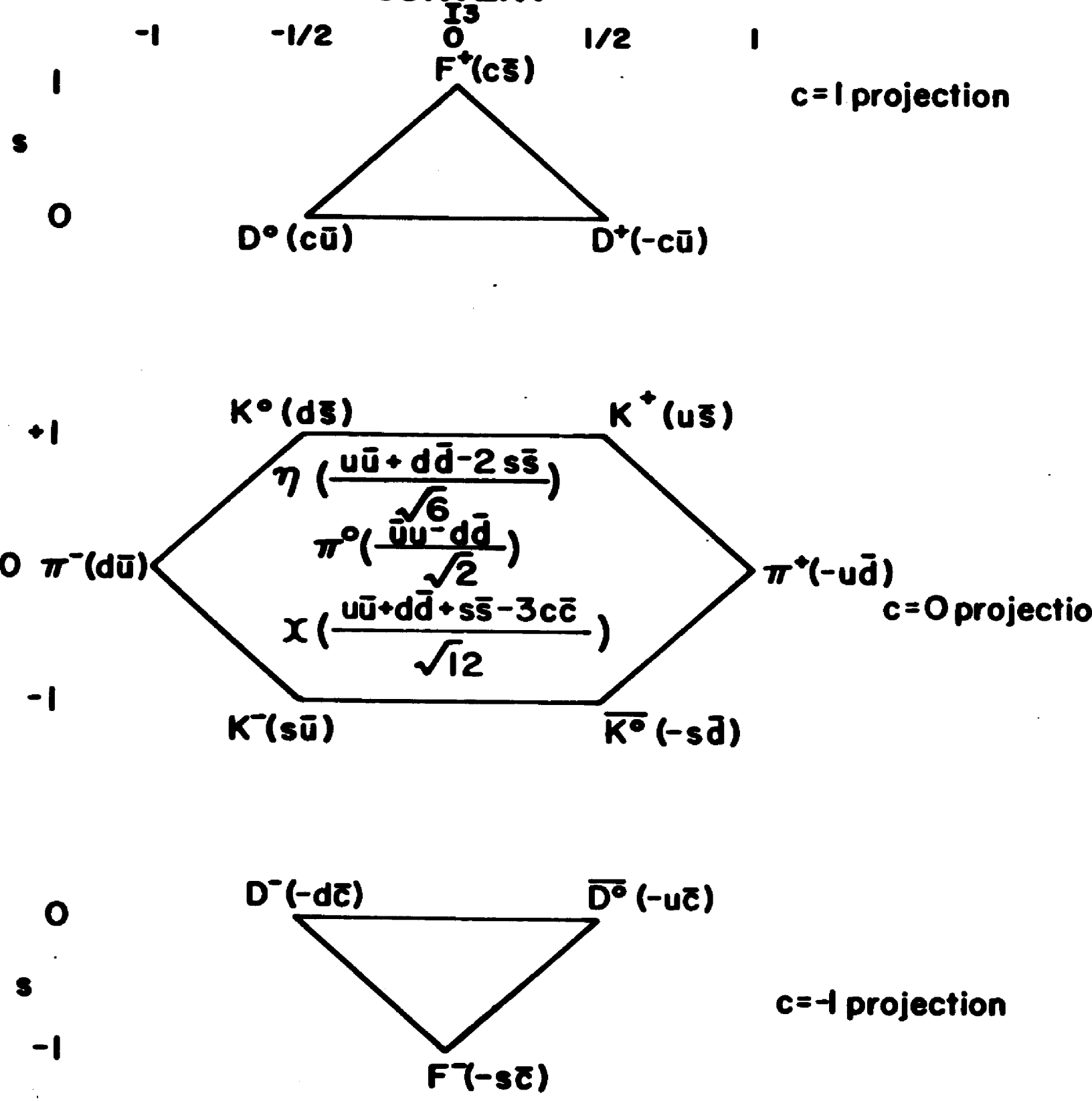

Although the neutrino experiments were seeing evidence of bare charmed decay, the e+e- machines were the first to observe the new mesons directly. Sitting slightly above the threshold for e+e- -> DD the SPEAR groups (16) determined the major decay modes of the pseudo-scalar D+(1867), D⁰(1863) mesons and the spin 1 excitation of these (cu), (cd) quark systems, the D*+(2010) and D*⁰(2008). Confirming the storage ring discovery, neon-hydrogen filled bubble chamber exposures in the Fermilab neutrino beam observed Kππ events in conjunction with an exiting muon at the same mass as the SPEAR signal (17).

A charmed baryon was first seen in the Brookhaven bubble chamber in 1975, (18) and a number of experiments at the ISR (19) have reported on charmed baryon signals within the last two years. Recently the Λc(2285) has also been seen at SPEAR (20). At this time only two electronic counter groups have reported a signal indicating production of the "F" meson (21) which is an isospin singlet consisting of a charmed and a strange quark. It has also been observed in neutrino induced emulsion events (22) events.

In 1977 a new family of vector mesons with narrow width at approximately 10 GeV was discovered at Fermilab (23) indicating that a heavier quark than charm was present. There have been no confirmed observations of hadrons carry-

ing the quantum number of the new quark designated "b" , as yet; nor has the b quark's presumed weak doublet partner, the "t" quark been seen at c.m. energies up to 31.6 GeV (24).

TABLE 1

Quark Properties

flavor	charge	baryon number	spin	quantity conserved by strong interaction
u	2/3e	1/3	1/2	isospin=1/2, I^3 = 1/2
d	-1/3e	1/3	1/2	isospin=1/2, I^3 =-1/2
s	-1/3e	1/3	1/2	strangeness =-1
c	2/3e	1/3	1/2	charm = 1
b	-1/3e	1/3	1/2	bottom = 1
t ??	2/3e	1/3	1/2	top = 1

Within the past year, measurements of the branching ratios for semi-leptonic decay at SPEAR have shown that the charged D meson has approximately 4-5 times the lifetime of the neutral D, assuming that the Cabibbo favored I=0 weak charged current in the GIM mechanism gives them equal semi-leptonic decay widths (25). This has called into doubt the previous picture of only the c quark coupling to the weak interaction vertex with the light u or d quark only behaving as a spectator to the process.

A whole new family of mesons and baryons had been discovered, but experiments in hadron beams remained unable to see any of them except for the J/ψ through the di-lepton decay mode because of the easy identification of energetic leptons. The problem of identifying hadronically produced charm that was forseen in the GIM paper, has been resistant to experimental solution.

Chapter II

CHARM HADROPRODUCTION PREDICTIONS

Production of particles containing massive quarks has been regarded as a process for which perturbative QCD can make reasonable predictions. The threshold at high energy for producing charmed valence quarks gives a known starting point for a perturbative expansion of the hadron fragmentation fragmentation functions into charmed particles and other Q dependent quantities. This situation for particles containing heavy quarks is markedly different from previous hadronic physics, where particle production can be explained fairly well by exchange of particles lying on Regge trajectories, but descriptions in terms of the underlying QCD field theory are much more difficult because of the ease with which new light quarks are created.

Most theorists give an estimate of 1 - 50 μb for the production cross section for charmed particles at Fermilab energies. Only the motivation for these estimates will be discussed instead of the detailed methods used to derive them. The free nature of the coupling parameters in QCD along with the sparse and sometimes contradictory data on the dynamically defined quark masses and parton distribu-

tions allow for much leeway in the final cross sections obtained.

Most models assume that hard scattering of the hadronic constituents gives the large momentum transfers leading to DD production in the central region. At least one experiment that will be discussed in Chapter VII casts some doubt on this assumption. The major contibuting QCD Feynman diagrams of lowest order in $\alpha_s = 12\pi/25\log(Q^2/\Lambda^2)$ include quark annihilation (Fig. 2 b), charmed sea quark excitation (Fig. 2 f-i), and gluon fusion (Fig. 2 c-e).

A group at Harvard (Georgi, Glashow, Machacek, and Nanopoulos (26)) considered most of the simple sub-processes that could contribute to charm hadroproduction. In their analysis they did not see a way to separate charmed quarks that bind together to form the charmonium states and charmed quarks producing D and $\bar{D}$ mesons or charmed baryons. They do state, in accord with Ioffe (27) that an excitation process that promotes charmed quarks out of the sea and onto mass-shell cannot be a major contributor - the charmed sea distribution has insufficient pairs. Simple light quark annihilation models predict a $1+\alpha\cos\theta$ distribution for the lepton pairs from the decay of hadronically produced J/ψ's, where θ is the angle relative to the incident beam direction. Two measurements find a value for α consistent with

Figure 2

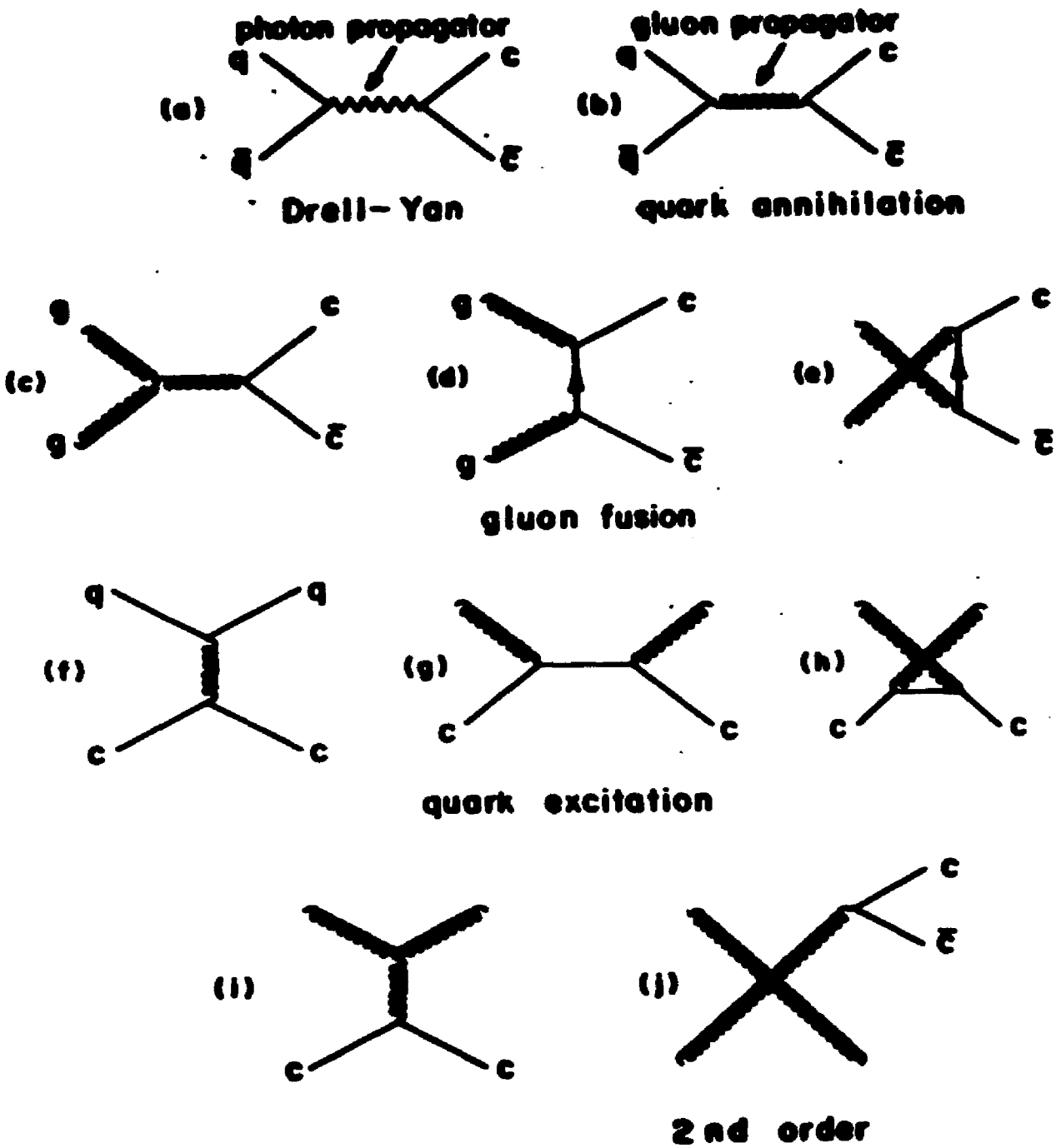
CHARM PRODUCTION FEYNMAN DIAGRAMS
photon propagator
gluon propagator
(a)
(b)
q
c
Drell-Yan
quark annihilation
g
(c)
(d)
(e)
gluon fusion
(f)
(g)
(h)
quark excitation
(i)
(j)
2nd order

zero. (28) Ioffe also predicts that heavy quark annihilation would give

$\sigma(AB->\psi' X)/\sigma(AB->\psi X) = [\Gamma(\psi'->e+e^-)/M^3(\psi')]/[\Gamma(\psi->e+e^-)/M^3(\psi)]$ = .27±.04, as opposed to the experimental determination of .05 - .12 for this ratio. In view of these results the authors above emphasize the importance of gluon-gluon interactions in producing charmed particles. The gluon-gluon interactions give rise to even parity, P wave states since the gluons have spin 1. Recent results from the Goliath apparatus at CERN and an ISR measurement (29) would appear to support this prediction; many of the observed J/ψ's were in coincidence with a photon from the decay of one of the C-even, P wave states of charmonium.

Combridge takes an opposite view and concludes that a flavor excitation from the sea qc->qc or qc->gc can be a major component of charm hadroproduction. He cited the work of Buras and Gaemers, (30) in determing the parton form factors from eN and νN inelastic scattering and found that though the charmed sea is very small at low momentum transfer it increases rapidly with Q^2. Combridge uses modified structure functions with a somewhat flatter gluon contribution, obtained from high mass di-muon production, assuming that process is dominated by the Drell-Yan quark-antiquark annhilation mechanism. With these assumptions he finds production dominated by flavor excitation diagrams at energies

not very far above threshold. Unlike the Harvard group he also assumes that the majority of charmed quarks will form mesons with bare charm once above threshold for the process. Because of the small contribution of quark annihilation there is little advantage to using beams of particles with valence anti-quarks, except near threshold. Combridge estimates that $\sigma(\pi p \to c\bar{c}+X;s) = 1/3\{\sigma(p\bar{p};3/2s) + \sigma(pp;3/2s)\}$ on the basis of the pion containing partons fewer in number but at higher average momentum than those in the nucleons. He finds this formula is in accord with similar results from high P_T π^0 production.

Another analysis of the question by Gluck, Owens and Reya (31) supports the Glashow group on the importance of gluon-gluon fusion. They find that quark annihilation or excitation out of the sea require a much flatter x distribution in the charmed sea than deep inelastic scattering data will support. They observe that all three diagrams of this nature (Fig. 2 c,d,e) are required for SU(3) gauge invariance. Instead of using the Buras and Gaemers structure functions Gluck and Reya calculated their own for nucleon targets and likely incident beam particles, (32) deemphasizing the Q dependence of the valence quark distributions.

These predictions of heavy quark production in QCD all convolute the parton distributions with the cross section

for the individual subprocess and integrate from threshold, $x_1 x_2 s = 4M_0^2$ to $x_1 x_2 = 1$. It has been pointed out that this description of s channel resonances and background in terms of the crossed channels of t and u for the sub-process was carried over from the Reggeon exchange model into parton physics. Production estimates near threshold using this duality concept should be viewed with some caution. The charmed quark pair may form bare charmed particles in the final state even if the s for the process was below $4M^2$ by combining with spectator quarks from the initial state (33).

R. Field pointed out that the assumption of first order diagrams ignores diagrams proportional to log Q. The four gluon vertex in Fig. 2(j) is an example of such a second order process. Another process not generally considered is hard scattering of light quarks that pull in a charmed quark from the sea to form a color singlet.

All of the preceeding references have assumed a central production with hard scattering of partons to dominate charmed meson production. Brodsky, Hazer, Peterson, and Sakai recently proposed a different model (34) to explain the large production cross sections measured away from the central region at ISR. They take the .1 - .5 mb cross section in the diffractive region to be an indication of a substantial cc component as an intrinsic constituent of the

nucleon instead of these pairs arising from quantum fluctuations. These charmed quarks are hypothesized to be at higher x than the lighter quarks, $\langle x\rangle=2/7$ as opposed to the $\langle x\rangle=1/7$ of the light quarks. Using these results in a simple production model Λc's and D 's are expected to be produced with $\langle x\rangle=4/7$ and $\langle x\rangle=3/7$ respectively. Brodsky et al. view production of charmonium states, which measurements show is central in character, to be a different process requiring the $c\bar{c}$ pair be nearly coexistent in phase space for a bound pair to form.

Rosner has given some estimates for the production ratios of the charmed particles in the limit of exact SU(3) global symmetry, without looking at the specific production mechanisms or absolute cross sections. Based on the spin degrees of freedom he predicts that at energies away from threshold for charm production the mesons will be directly produced in the ratio $F^{*+}:D^{*+}:D^{*0}:F^{+}:D^{+}:D^{0} = 3:3:3:1:1:1$ and the charmed baryon cross section will be $1/5<\sigma(Bc)/\sigma(D)<1/3$. The observed branching ratios for D* decay are $BR(D^{*+}\to D^{0}\pi^{+}) \sim .6$, $BR(D^{*+}\to D^{+}\pi^{0}) \sim .3$, and $BR(D^{*0}\to D^{0}\pi^{0},\gamma) = 1$, so one expects approximately 1.9 D^{0} per D^{*+} in the final state. If the production rates for these mesons are equal the ratio of $D^{0}:D^{*+}$ goes up to 2.6, indicating that the branching ratios in D* decay force the D :D* ratio to about two and it is relatively insensitive to the exact production ratio. This

allows a comparison of the results of this experiment, sensitive to the charged D*'s, with other experimental measurements with some confidence.

Because of close dependence on the underlying field theory of interacting fermions and bosons the phenomenology of hadrons containing heavy quarks will in all likelihood be different from that of hadrons containing light quarks. Conflicting predictions for charm hadroproduction will only be resolved by experimental determination of the energy and beam particle dependence of the cross section along with the Feynman x and P dependence. Detailed studies of the differential cross sections as a function of the kinematic variables of inclusive production will require a new generation of experiments; at the present time observing any charm mass signal is a major challenge.

Chapter III

PREVIOUS HADRONIC CHARM SEARCHES

Positive results of hadronic charm production searches have been reported by groups looking for three entirely different signals: a peak in an invariant mass distribution, prompt lepton production from the semi-leptonic decay of charmed mesons, and the appearance of short lived (10^{-12} - 10^{-14} second) particles in high resolution optical track detectors. In general all hadron beam charmed meson experiments, including this one, survey only a limited set of the possible charm decay products, or a small region of the decay phase space, or both. Hence in drawing conclusions about total cross sections from their results, assumptions must be made about the cross section's dependence on kinematic variables or the decay rates of the charmed particles into various final states.

Cross sections quoted from reports on these searches have been adjusted where necessary to take into account the latest measurements of branching ratios and lifetimes. An overall semi-leptonic decay ratio of 8% for neutral and charged D's is obtained from the individual decay ratios of 5% and 18% respectively, in conjunction with Rosner's pred-

iction described earlier of three times as many D^0's as D^+'s in the final state. The preponderance of leptons associated with charm decay is assumed to come from D decay modes.

There have been three generations of prompt lepton experiments. Two of the first generation experiments measured the ratio of electron to pion production at 90° in the c.m. as a function of transverse momentum. An experiment at Fermilab took data on muons produced in 300 GeV/c proton interactions using a single arm spectrometer and several hadron absorbers that allowed differentiation of the prompt signal from the hadron decay muons (35). An experiment at the ISR observed electrons directly produced in pp collisions at $\sqrt{s}$ = 53 GeV with two electron spectrometers located opposite to each other and at 90° in the c.m. (36). An analysis of these experiments by Bourquin and Gaillard (37) indicates that the lepton to pion ratio measurements at low P_T cannot be accounted for by known sources of leptons in hadronic collisions. This leads them to infer a charm cross section of 12 μb for DD production at $\sqrt{s}$ = 20 GeV. The lack of data in the P region below 1.5 GeV/c for the Fermilab data and the large error bars on the ISR data do not allow a convincing argument for charm production.

In one of the latest prompt lepton searches a series of experiments was conducted in the CERN SPS neutrino beam

observing neutrinos produced in a copper target which was thick enough to absorb nearly all hadronic secondary particles. The copper plates could be separated to give a variable density target. Linearly extrapolating data points taken at several plate separations to infinite density allows the "prompt" signal, that is unrelated to more ordinary decays, to be extracted from the data. The latest data in this beam dump type experiment were taken in 1979 with a 400 GeV proton beam. Particular attention was given in this run to suppression of background from decays not coming from the target. Experimental data was taken with three separate detectors in the neutrino beam simultaneously. There was a 3.7 m. bubble chamber filled with a neon-hydrogen mixture and operated in conjunction with an external muon identifier. This was followed by a detector consisting of 500 tons of magnetized steel instrumented for the analysis of reaction products from neutrino events (38). The third apparatus consisted of a 100 ton marble calorimeter and toroidal magnet muon spectrometer (39).

Wachsmuth has analyzed the preliminary results from the three data samples (40), to get a consistent result for a model dependent cross section for charm production. The ratio of ν_μ to ν_e detected was almost 2:1 instead of the unity expected from the semi-leptonic decay of charmed mesons. This possibly was caused by systematics in the

background. There is also a 3:1 asymmetry in the ν's to $\bar{\nu}$'s detected in the bubble chamber and magnetized steel detectors, as opposed to the 2:1 interaction cross section ratio. Wachsmuth believes this to be an indication of charmed baryon production with nearly flat x dependence. Assuming a 5% semi-leptonic branching ratio for all charmed hadrons the three experiments get charm cross sections of 44±12 μb, 24±10 μb, and 50±10 μb respectively from the $\nu_\mu, \bar{\nu}_\mu$ data. The bubble chamber experiment was able to detect ν_e events directly and measure a prompt signal that corresponds to a 22±6.4 μb charm cross section. Wachsmuth believes this to be the most reliable charm signal of the prompt neutrino measurements.

Experiments looking for a prompt muon signal have been conducted at Fermilab using a target made of steel plates with expandable spacing and interleaved with scintillation counters for determing the energy in hadronic showers produced in the target. The latest data sample taken using this target observed muons in a modular steel range detector and toroidal steel muon spectrometer. The apparatus could detect nearly all muons with x>0 and E>8 GeV, minimizing the dependency of cross section normalization on production models. With an acceptance of 39% for single prompt muons from charm decay a total cross section of 22±9 μb is obtained for 350 GeV/c p-Fe interactions (41). An earlier

version of the experiment without the muon range detector was run with a 400 GeV proton beam. It was triggered on a μ^+ with $P_T > 1$ GeV/c to minimize contamination from well understood sources of muons, as suggested in the Bourquin and Gaillard analysis of previous experiments. Single prompt muon data from this experiment gives a $\sigma_{TOT} = 21 \pm 5$ μb and muon pair data, requiring a more model dependent interpretation, gives 14 ± 3 μb. The cross section values obtained from the single muon and muon pair data are not inconsistent with each other. Associated production of F mesons, Λ_C's, and other charmed baryons may well account for 1/3 of charm pairs, and these other charmed hadrons will have smaller semi-leptonic branching rates than the lowest mass D's. A branching ratio of 5-6% for all charm into leptonic modes is in accord with the data (42).

In a second generation prompt lepton experiment at the ISR two electron and one muon spectrometer at 90° to the colliding beams were used to look for evidence of DD production. An analysis of the data samples of ee and eμ pairs give $d\sigma/dy = 15 \pm 3$ μb at $y=0$ (43) for pair production of charmed mesons, assuming the meson pairs are responsible for the entire prompt lepton signal.

Examining cosmic ray events in emulsions, Gaisser and Halzen estimated a charm cross section of 30 μb (44) at

Fermilab energies. Recent experiments using high resolution optical detectors have attempted to identify charm events in the same manner, by the characteristic decay vertex of these particles which travel a measurable distance before decaying. The strange particles were similarly discovered 25 years earlier by the "Vee" signature in cloud and bubble chamber events.

In an initial attempt at detecting charm decays optically an emulsion stack was exposed to 400 GeV/c protons at Fermilab. Out of nearly 1700 interactions seen in the emulsion scan two appeared to show the production and subsequent decay of a pair of neutral charmed particles. A charm cross section of 30±20 μb was inferred from these two events by the experimenters (45). A high pressure streamer chamber in a 350 GeV/c proton beam at Fermilab was triggered on an exiting muon. The experimenters reported ten events above the predicted background satisfying their event selection criteria. Interpeting these events as charmed meson decays gives a charm cross section of 20-50 μb (45) for a D lifetime of 10^{-12} seconds. At CERN a very small, rapid cycling bubble chamber was exposed to a 340 GeV/c pion beam. The photographic system was triggered when bubbles had expanded to only 40-50 μm, giving the resolution required. The film was scanned for track geometries consistent with the hypothesis of associated production and subsequent decay of a

charmed hadron pair. Twelve events more than the predicted background were observed, implying a charm cross section of 40 μb (47) assuming a D lifetime of 5×10^{-13} sec . None of these experiments had momentum analysis of the decay particles and the bubble chamber and emulsion experiments lacked any particle identification.

All of the experiments described give evidence for the production of charmed mesons but cannot definitely ascribe their signal to this source. There have also been experiments that have looked for peaks in an invariant mass distribution at the D mass. The only experiment with data that indicates a mass peak with over 4σ significance utilized the Split Field Magnet at the ISR (48). Data from this apparatus were analyzed for signs of the decay $D^+ \rightarrow K^- \pi^+ \pi^+$, with the requirement that the mass of one of the $K\pi$ pairs fall within the $\overline{K^{*0}(890)}$ resonance. The use of this constraint was motivated by the observation that half of the semi-leptonic decays of the D are into the K*. Additional cuts on the data were made by requirements on the x and P_T of the triggering K^- meson and on the recoil particle systems. This analysis gives a five standard deviation peak in the $K\pi\pi$ mass centered at 1.91 GeV leading to a σ_{TOT} of 150 μb for a flat x distribution and 830 μb for a $(1-x)^3$ production distribution. An assumption was made that 2/3 of the $K\pi\pi$ decays goes through the $\overline{K^{*0}}$ channel, for a branching ratio

of 2.6±1 %. Dalitz plots of D+-> Kππ decays from SPEAR data fail to support this assertion, and set an upper limit of 15% for the K* decay mode. (49) If one applies the SPEAR results, the cross sections obtained from the SPM experiment's data increase by a factor of four, making them difficult to reconcile with other experiments.

The experiment most similar to the present one was conducted by a Fermilab-Michigan-Purdue collaboration (50) in a 400 GeV proton beam at Fermilab. They used a double arm spectrometer in an attempt to see the Kπ decay from D's produced in a thin segmented target. The apparatus had excellent mass resolution (8.5 MeV at 2 GeV and 12 MeV at the 3.1 GeV J/ψ mass) but failed to find a significant peak even with ~ 10K events per 10 MeV/c^2 mass bin in the Kπ invariant mass plot. Using a 4σ criterion this experiment set an upper limit on the D cross section of 76 μb. In their report the experimenters concluded that brute force techniques were not likely to succeed in enhancing the signal to noise ratio in invariant mass plots because of the combinatoric background from the non-charmed hadronic processes that have a cross section at least a thousand times greater. A way of enriching the charm signal would have to be found.

An experiment with an enrichment technique was performed at Brookhaven with a three arm spectrometer looking for D*'s from exclusive associated production of a charmed baryon, Bc, near threshold with a mass of roughly 2.6 GeV. The third arm was installed to detect the low energy pions that would be produced nearly at rest in the c.m. from the D*+-> $D^0\pi^+$ decay, while the other two arms viewed the $K\pi$ decay of the D as in the previously mentioned experiment. The third arm requirement decreased the trigger rate by a factor of fifty and offline analysis requiring the Q-value for the D* decay be consistent with the 5.7 MeV value measured at SPEAR gave a further factor of three improvement in signal to noise despite the crude (±5 MeV) Q-value resolution from the third arm. Based on a 4 standard deviation criterion an upper limit of 5.1 μb for $\sigma(\pi N \rightarrow D^{*-} + X)$ was deduced (51).

A recent report of charm photoproduction observed in the Fermilab wide band photon beam (52) shows the validity of this approach. A very clean 7 standard deviation signal in $D \rightarrow K\pi$ is observed by looking for $D^* \rightarrow D^0\pi$ decay and then requiring that $3<Q<8.5$ MeV for this reaction. Without this Q-value cut the $D^0 \rightarrow K^-\pi^+$ signal has a three standard deviation significance.

Chapter IV

THE SPECTROMETERS

In order to search for D* hadroproduction at Fermilab energies we constructed the three arm spectrometer apparatus shown in Fig. 3. It was constructed with two identical narrow acceptance arms capable of analyzing and identifying particles with momentum from 5 - 30 GeV/c and a third arm with nearly 100% acceptance for particles from 1-3 GeV/c emitted within a 50 mrad cone about the incident beam direction. u The two spectrometers for analyzing the high momentum particles were designated Left and Right, looking downstream from the experimental target. The fast arms had two Cerenkov counters, one CO_2 threshold counter and one FREON 114 differential counter, both at atmospheric pressure, for K-π-p separation. Segmented steel muon filters following these two arms enabled muons to be identified and thus allowed the use of J/ψ production and decay to monitor beam flux and calibrate the mass scale of the two fast arms. The slow arm had no particle identification. The results of Monte Carlo studies of acceptance of decay products as a function of the P_T and x of the parent D* are shown in Fig. 4. These studies indicated the optimum acceptance for the fast arms was at an opening angle of 150 mrad. Assuming

Figure 3

E567 APPARATUS LAYOUT

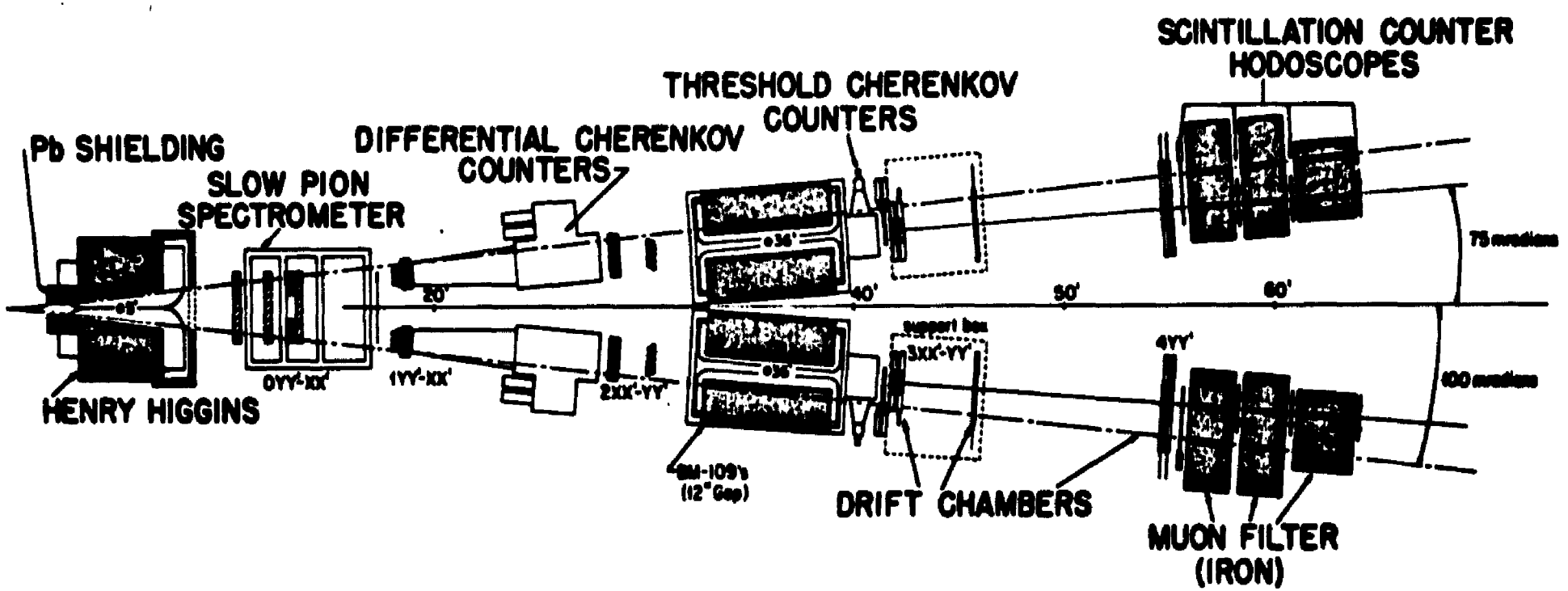

an invariant production cross section proportional to $(1-|x|)^3 \exp\{-1.1P_T^2\}$ a total acceptance of $3.5\pm.1 \times 10^{-4}$ is obtained from the Monte Carlo.

The two arm design with small acceptance reduced the probability of more than one particle being present in either fast arm per interaction. This allowed particle identification with little ambiguity both for the fast trigger logic and in later off-line analysis. Space limitations dictated the construction of shorter spectrometer arms than were used in the Fermilab-Michigan-Purdue experiment. This resulted in a mass resolution only half as good for the two body D^0 decay in this experiment. However, the resolution of the D^* decay Q-value was nearly an order of magnitude better than the previous experiment at Brookhaven, which did not have wire chambers in the third arm. A .5" (.03 nuclear absorbtion length) beryllium target was used to minimize multiple Coulomb scattering within the target that could degrade Q-value resolution below the inherent resolution of the apparatus.

The analyzing magnets for the fast arms were Fermilab BM109's, which had 72" long poles and an aperture opened to 12" x 24". Flux returning shield plates were installed on both the upstream and downstream ends of these magnets. They were cabled in series and excited with 2450 A during

Figure 4

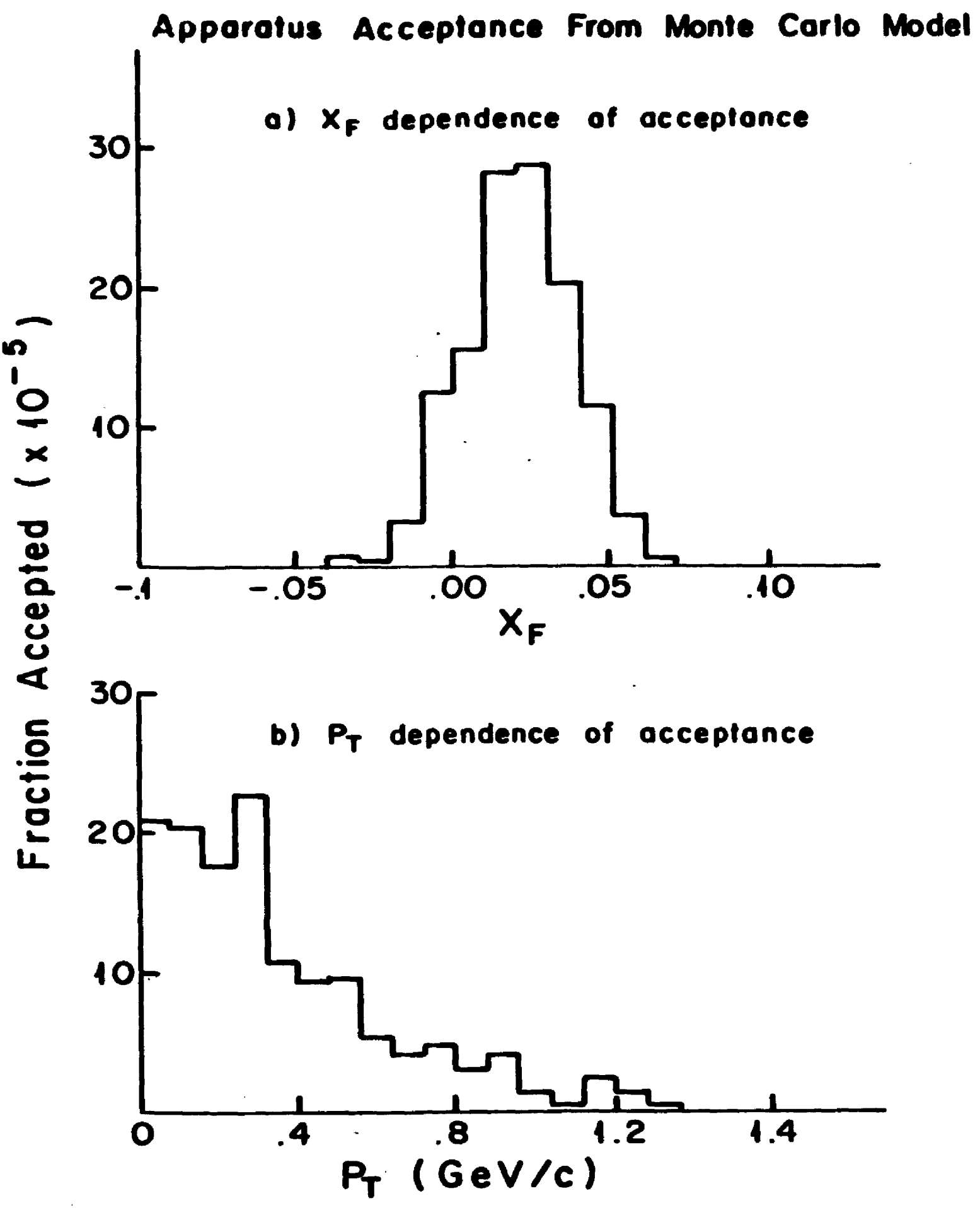
Apparatus Acceptance From Monte Carlo Model
a) X_F dependence of acceptance
30
20
10
-.1
-.05
.00
.05
.10
X_F
Fraction Accepted ($\times 10^{-5}$)
b) P_T dependence of acceptance
30
20
10
0
.4
.8
1.2
1.4
P_T (GeV/c)

the entire run. Flip coil measurements made at this current gave flux integrals of 850 kG-in., corresponding to a $P_\perp$ of 650 MeV/c. These measurements were within a percent of the values obtained from fits using data containing well known resonances. Variations in the $P_\perp$ from these magnets caused by inhomogeneities in the field were fit to a form, $B\cosh(y/a)\cos(x/a)$, established by detailed studies done by a Fermilab group. Fits of field measurements of the BM109's in this experiment gave values of B =-.0012 MeV/c, and a = 2.6" . The field deviations for the track positions at the entrance and exit of the BM109 were averaged to form the correction applied to the data, with a maximum correction of about 1.8% to the $P_\perp$ of the BM109. The slow arm magnet was obtained from Brookhaven National Laboratory (labeled Henry Higgins for unknown reasons). It was a 48" dipole with 22" x 34" aperture. A flux return plate was installed only on the downstream side of this magnet, and a lead collimator with steel sides was inserted into the field volume to prevent the slow arm from directly viewing the target. These two factors caused the magnetic center to be offset from the center of the pole pieces. Henry Higgins was excited with 780 A giving a field integral of 600 kG-in., equivalent to a $P_\perp$ of 408 MeV/c. All three magnets were oriented to bend particles in the vertical (Y) direction. Both magnet power supplies were continuously monitored by the Fermilab Proton beam-line control system, and also monitored locally with a

digital voltmeter attached to 55 mV shunts in the power supplies.

Each fast arm had five hodoscopes for all tracks plus a pair of counters located behind each of the three muon filter segments. Four of these hodoscopes were required in the fast trigger logic and were used for track reconstruction. The fifth hodoscope was tilted 26.5° from the vertical, giving a stereoscopic view for matching X and Y track views when more than one track was found in an arm. Both Y viewing hodoscopes were located after the analyzing magnet and were used to determine a particle's sign and make a rough momentum selection. The two X viewing hodoscopes were located in front of the first Cerenkov counter and behind the analyzing magnet respectively forming a long road for the track reconstruction program. All hodoscope scintillators in the fast arms were contructed of 1/4" plastic scintillator material (NE110) and used RCA 8575 (or functionally equivalent) photomultipliers. The tubes were run with a negative high voltage set to give a peak for minimum ionizing particles of 120 mV into 50Ω, an operating point determined by plateau curves taken for each hodoscope. The muon scintillation counters used RCA 6655 photomultipliers that were run with positive high voltage.

There were two atmospheric pressure gas Cerenkov counters in each fast arm. The light collecting optics of both counters were segmented to improve off axis collection efficiency. This segmentation, into independent upper and lower cells, reduced background counts and allowed particle identification when there was more than one particle present in an arm.

The CO_2 filled threshold counter was located in the BM109 analyzing magnet, conserving space and preventing low momentum electrons from interfering with its operation. It had a threshold near 5 GeV/c for pions and was thus used to separate pions of momentum greater than 5 GeV/c from other particles both in the trigger logic and in off-line analysis. The gas cell for the Cerenkov radiator was constructed from black phenolic to prevent eddy currents or vibration in this counter induced by ripple in the magnet power supply. A 10 GeV/c pion gave an average of 8 photoelectrons. The RCA 8854 5" photomultiplier tubes used to observe the Cerenkov light were operated with positive high voltage bases to minimize leakage currents from the tube envelope to the surrounding magnetic shields. Construction details for this counter may be seen in Fig. 5.

A differential counter of the type proposed by V. Fitch (53) was also incorporated into each fast arm, in front of

Figure 5

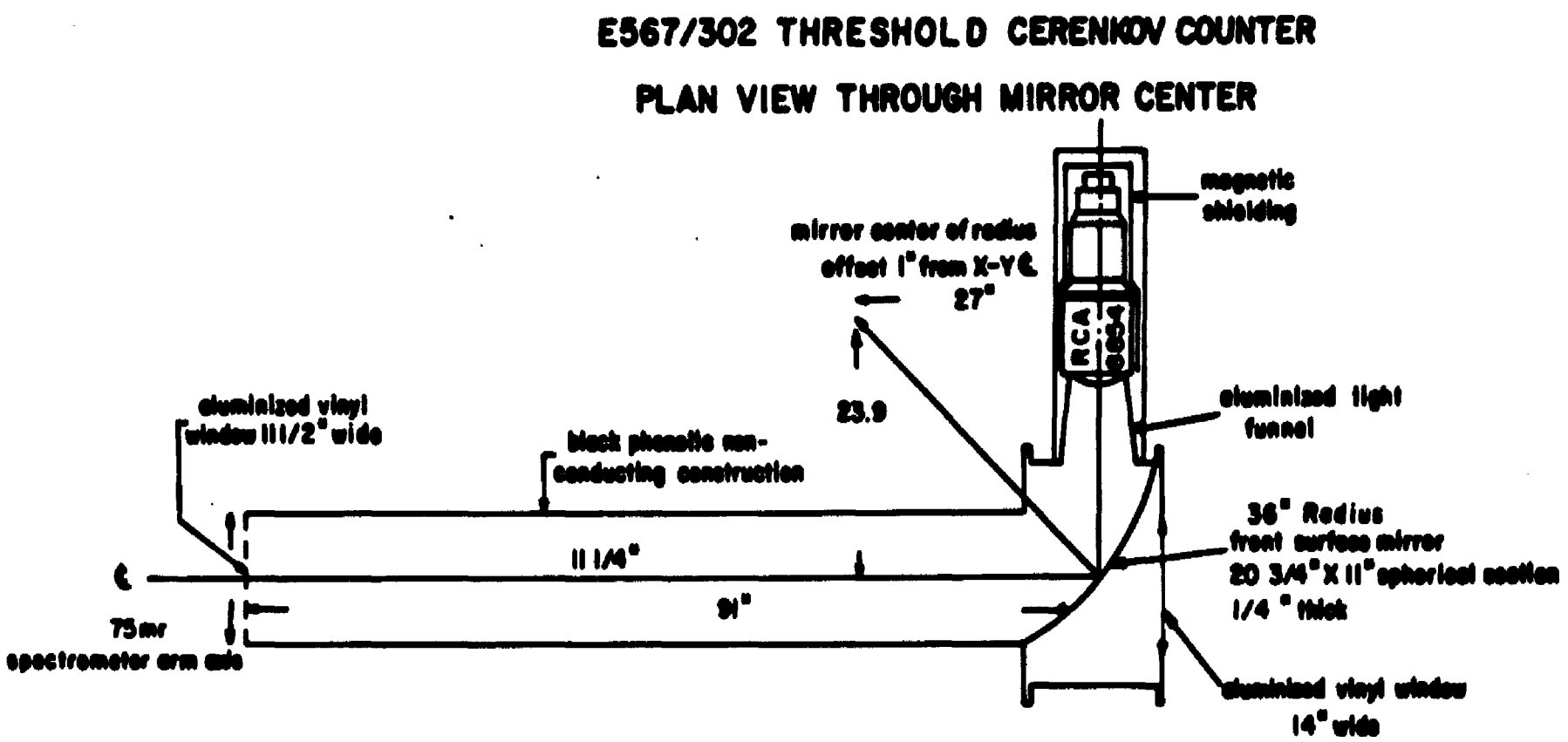
E567/302 THRESHOLD CERENKOV COUNTER
PLAN VIEW THROUGH MIRROR CENTER
magnetic shielding
mirror center of radius offset 1" from X-Y ℄
27"
23.9
RCA 8854
aluminized light funnel
aluminized vinyl window 111/2" wide
black phenolic non-conducting construction
36" Radius front surface mirror
20 3/4" X 11" spherical section
1/4 " thick
111/4"
91"
℄
75mr spectrometer arm axis
aluminized vinyl window 14" wide

the analyzing magnet. These counters were filled with FREON 114(dichloro-difluoro-ethane). Their threshold behavior allowed separation of protons from kaons above 11 GeV/c, and pions from kaons in the 4 -10 GeV/c region. FREON 114, although it has a large index of refraction (1.00135) and is non-flammable, had a disadvantage in comparison with high refractive index hydrocarbon gases that could have been used. Its chlorine content was the largest single source of multiple scattering in the fast arms, a price paid for safety.

To achieve the particle separation required in this experiment it was not necesary to use the differential features of this counter. Correspondingly, only the sum of the pulse heights from the photomultipliers was used to give a threshold signal. These counters were constructed of aluminum with vinyl windows. They used the same tubes and bases as the threshold counters. Differential counter optical layout and some construction details are shown in Fig. 6.

The drift chambers in the fast arms used a configuration with one sense wire and three drift wires between two ground planes as shown in Fig. 7. The 1/2" drift distance cells were used in chambers 0X and 2X, which were expected to have the highest rates. The field from this arrangement was investigated numerically and checked using teledeltos paper.

Figure 6

E567/302 DIFFERENTIAL CERENKOV COUNTER

PLAN VIEW

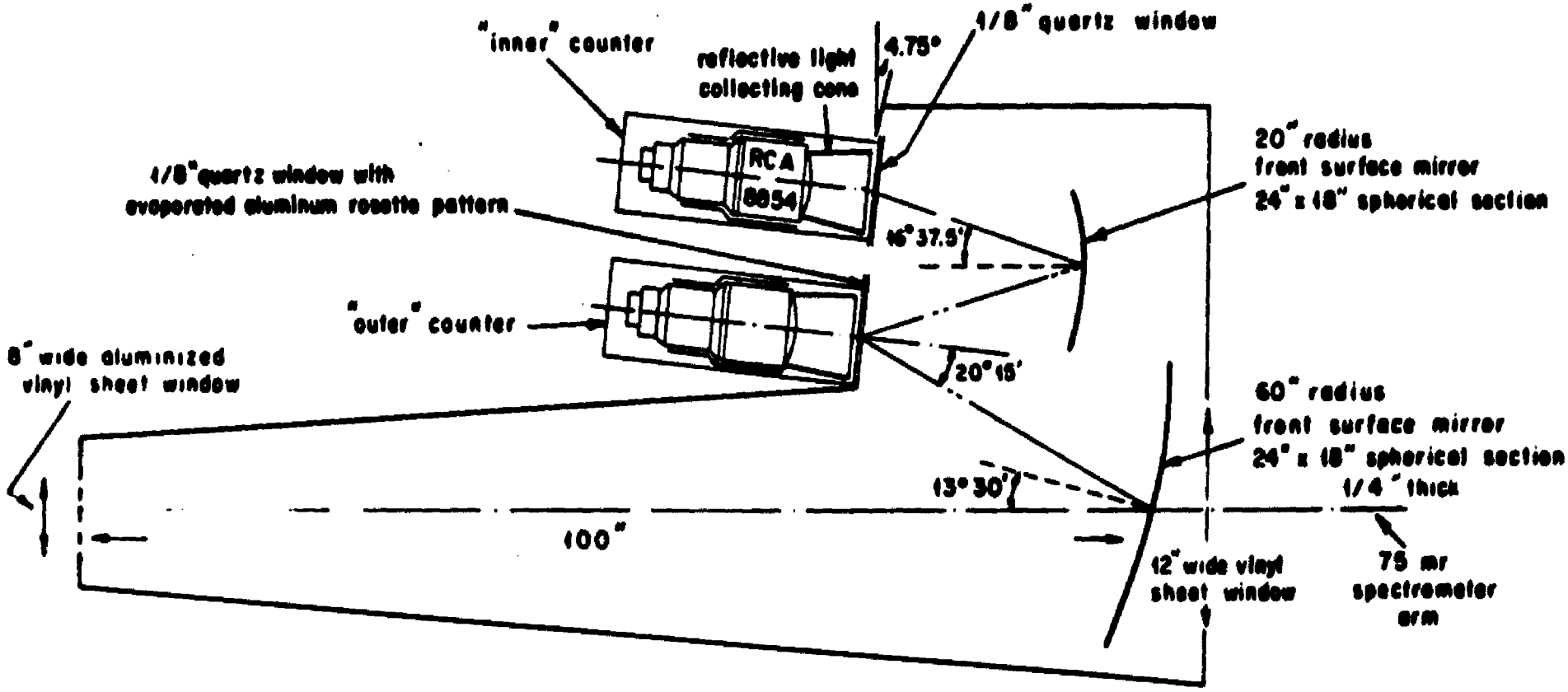

The chambers could be plateaued routinely to better than 99% efficiency with a beta source. There were no problems with efficiency or drift time linearity as shown in Fig. 8. Except for 3Y' each chamber had two planes, staggered by half a cell width to resolve left-right ambiguity.

All the chambers in the experiment were run on a 50-50% (by volume) mixture of argon and ethane. Results of tests published in reference (54) have shown this gas mixture to have good velocity saturation characteristics. The maximum drift time with this mixture was about 450 ns in the 1" cells. As a test, a chamber filled with the argon-ethane mixture was exposed to a high intensity beta source for two weeks. No degradation in efficiency was observed, showing there was no requirement to include hazardous solvents in the gas to prevent radiation induced polymerization of the ethane. The gas was mixed locally using Matheson 603 flowmeters and precision needle valves that had been checked for temperature sensitivity. Using the flowmeter calibration curves and the advertised accuracy of the individual flowmeters the the variation in the mixture is estimated to be less than 3%. There was a pressure alarm warning when gas flow in the chambers ceased but no monitor of the mixture ratio.

Figure 7

PRINCETON DRIFT CHAMBER CELL CONFIGURATION E302/567

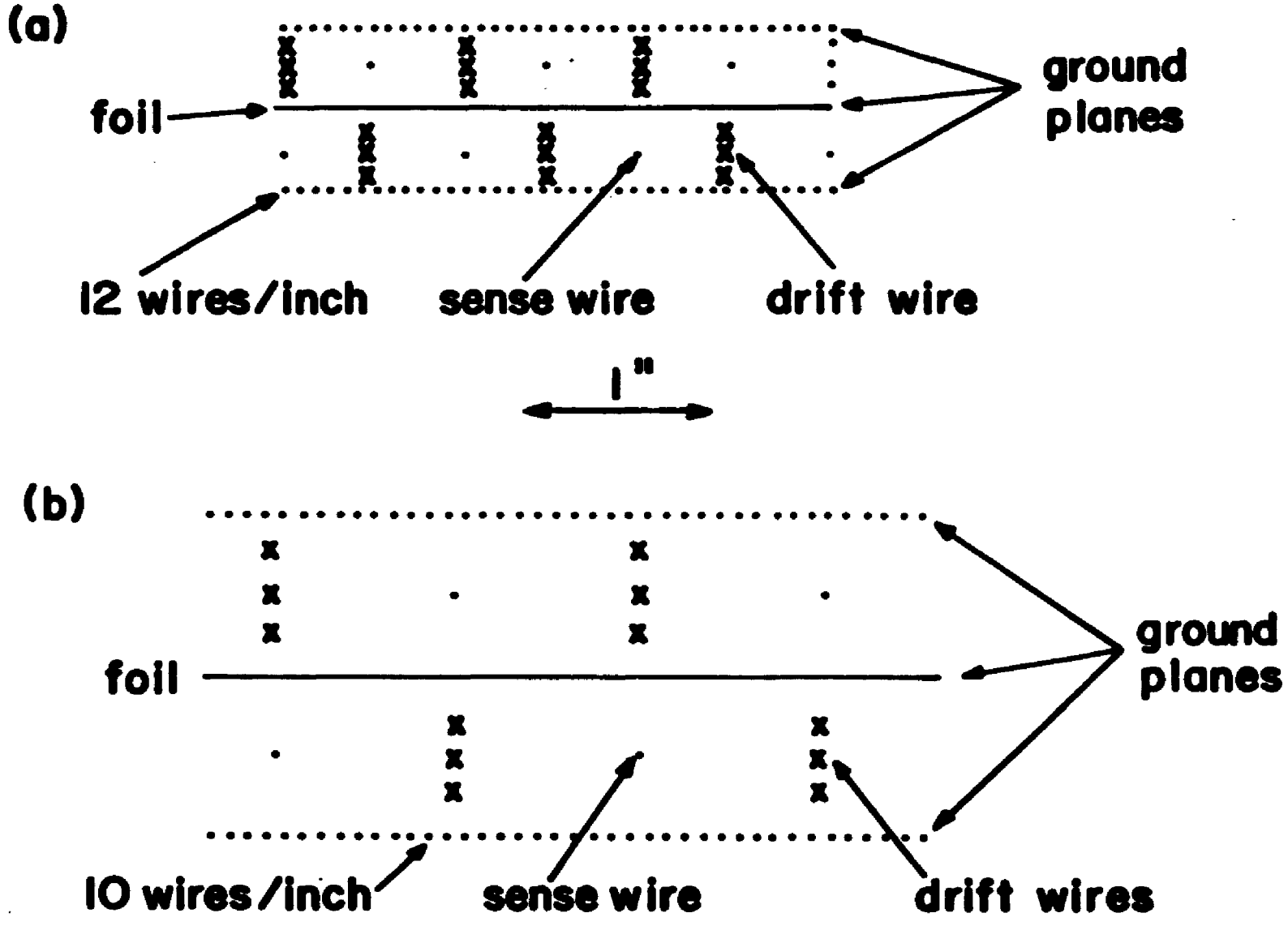

sense wires: .8mil gold plated tungsten
drift wires: 5mil Be-Cu
groundplane wires: 5mil Be--Cu

Figure 8

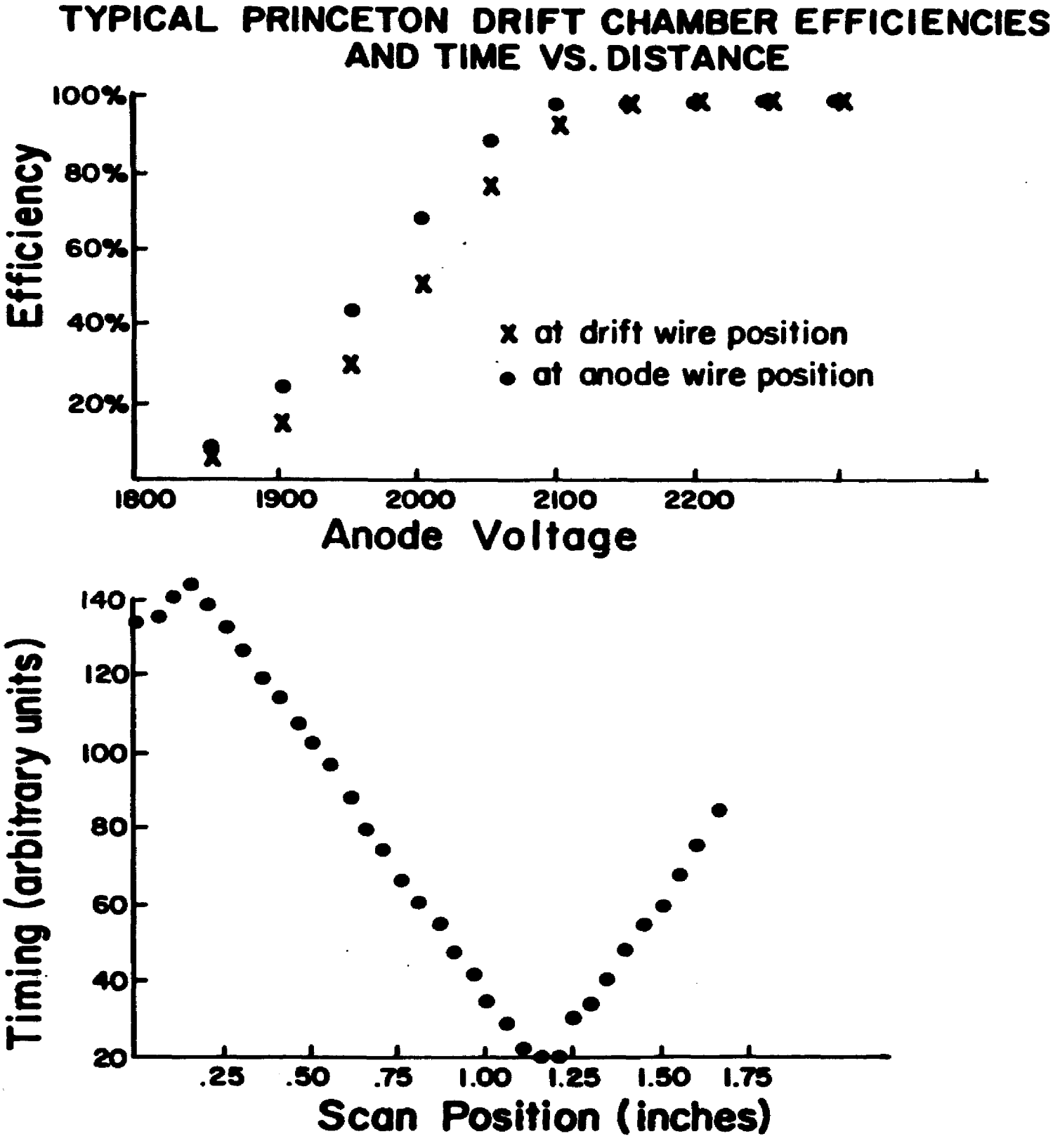
TYPICAL PRINCETON DRIFT CHAMBER EFFICIENCIES AND TIME VS. DISTANCE
Efficiency
100%
80%
60%
40%
20%
x at drift wire position
• at anode wire position
1800
1900
2000
2100
2200
Anode Voltage
Timing (arbitrary units)
140
120
100
80
60
40
20
.25
.50
.75
1.00
1.25
1.50
1.75
Scan Position (inches)

Figure 9

PRINCETON DRIFT CHAMBER AMPLIFIER

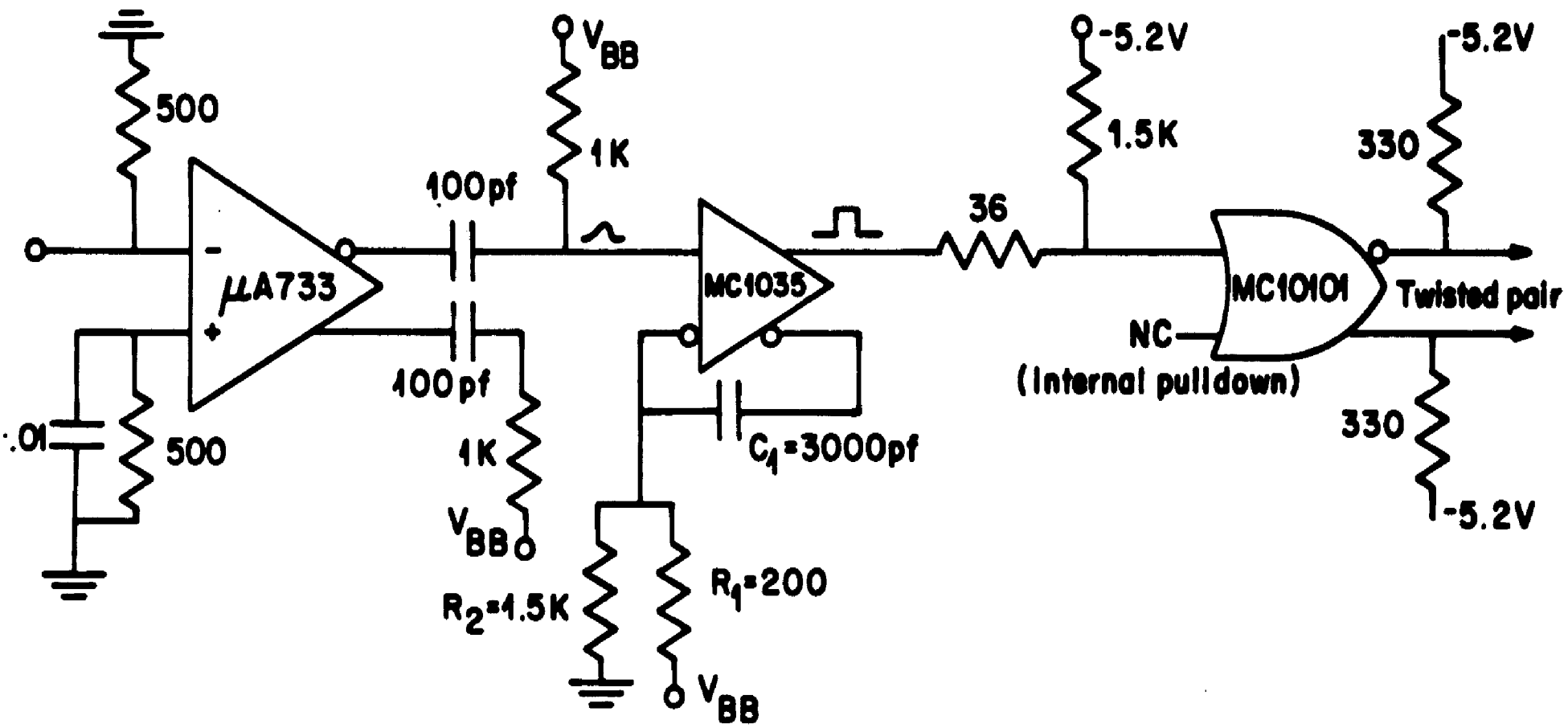

The drift chamber amplifier shown in Fig. 9 is a modification of the circuit described in reference (55). The dead time was increased to 250 ns after the pulse from the sense wire to eliminate circuit refiring that had been observed in previous operation. The output capacitors were bypassed and the output line driver terminated to -5.2V through 330Ω pulldown resistors to give the complementary ECL level signal required by the time digitizing system used by this experiment. The 733 video amplifier integrated circuits were vulnerable to sparking in a chamber, but under normal operating conditions the chamber mounted amplifier boards were trouble free.

A difficulty in the fast arm drift chamber system arose in the four separate chamber packages that constituted 4LY and 4RY, the largest chambers in the experiment. Although these chambers had a cell configuration identical to the other chambers with 1" drift regions, each displayed a markedly lower drift velocity than the 20 other chambers in the fast arms when all were operated at the same voltage. An obvious explanation, gas impurity, would also have caused a change in the plateau voltage, which was not observed. It was necessary to run these chambers at about 4100 V/in (as opposed to 3500V/in) so the drift times from these chambers would fall entirely within the range of the drift time digitizers. Since a separate calibration was made for each

chamber this was not an inconvenience. The fast arm drift chamber system had an accuracy of .028" point as determined by residuals from fits to straight through tracks.

All the components in the slow pion arm except the magnet were designed and constructed at Saclay. As shown in Fig. 10, the spectrometer was built in two symmetric segments about the horizontal median plane to analyze low momentum particles of either charge. There were two hodoscopes with horizontal elements in each segment. They were used in the triggering logic and the track reconstruction program. The eight elements in each hodoscope were sized and placed so that roads were formed pointing back to the center of the analyzing magnet. There were no hodoscopes in this arm giving information on the X-positions of the tracks.

The drift chambers used graded potential cells with two anodes per cell 1.5 mm apart to resolve left-right ambiguity in the hit location. The wires in the middle X chambers were tilted 7° from the vertical to facilitate matching tracks found in the X and Y views. Details of the contruction of these chambers may be found in reference (56), as well as the circuitry for their amplifiers, which were designed around the 10216 ECL line receiver. The drift chamber amplifiers used in this arm were separate from the

SLOW PION SPECTROMETER

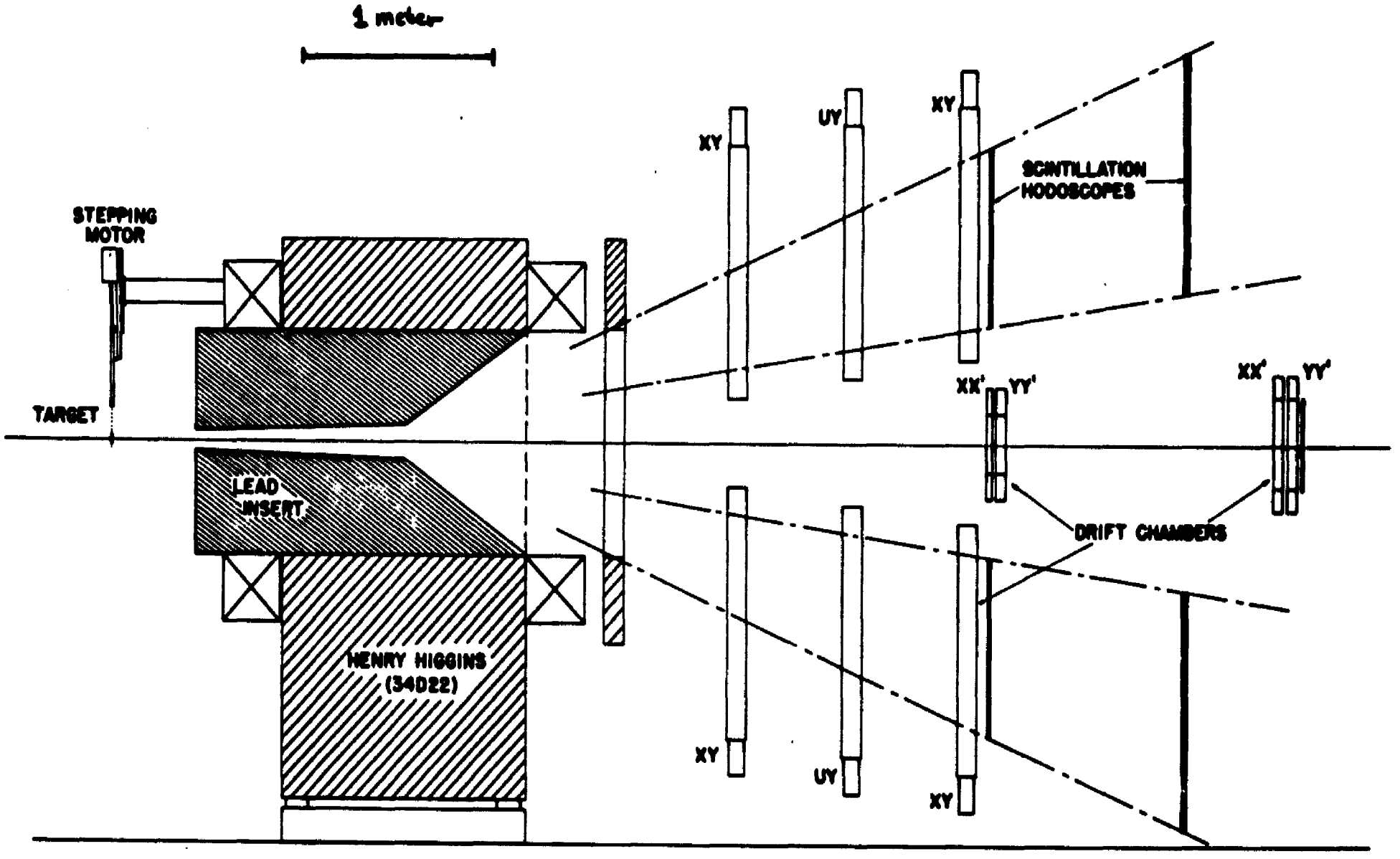

ECL line drivers so a capability of digitizing three hit times on a wire with one stop signal was readily implemented. This multiple hit capability was installed on the twelve wires in the slow arm which had the highest rates. Slow arm chamber resolution was determined to be .014".

All particles detected in this arm were assumed to be pions. The near equality of counting rates in the two segments, reflecting nearly equal numbers of positive and negative particles, indicates that proton contamination of the pion sample in the slow arm cannot have been too great, since many more p's than $\bar{p}$'s would be expected from the baryonic target. Inclusive production measurements at $\sqrt{s}$ = 23 GeV in p-p collisions give a p:$\bar{p}$ ratio of about 7:1 (57). However, mis-identified protons will contribute to the background to the desired reaction. It has been proposed that any future running with this apparatus implement either time of flight particle separation or an aerogel Cerenkov counter to separate pions from protons.

There was no particle identification of the incident beam since pions could be expected to form the vast majority of secondary particles from the production target, and the beam flux was to high to allow identification of individual particles. However a Cerenkov counter in the beam line filled with helium at half atmospheric pressure was used to detect

abnormally large particle bunches in the beam time structure, since the apparatus would not function well in the extremely high instantaneous rates sometimes extracted from the main ring.

TABLE 2

Spectrometer Hodoscopes

	number of elements	element size (in)	arm coordinate (from magnet) Z (in)	Y	photomultiplier tube
Fast pion-kaon arms					
PIX	6	1x20	-205	0	RCA 8575
PIIX	10+corners	1x20.25	-55	0	RCA 8575
BOX	8	1.5x30	69	0	EMI 9813KB
BIY	10	3x13	71	0	RCA 8575
BIIY	16	4.5x17	197	0	RCA 8575
μI	2	12x48	231	0	RCA 6655
μII	2	12x48	262	0	RCA 6655
μIII	2	12x48	293	0	RCA 6655
Slow pion arm					
UP (DOWN) TY	8	1.97,2.95,2.95, 3.98,3.98,3.98,3.98, 4.92x22.8	117	(-)90	AMP XP2020
UP (DOWN) TIY	8	4.53,5.91,5.91, 7.29,7.29,7.29,7.89, 9.85x22.8	157	(-)120	AMP XP2020

TABLE 3

Drift Chamber Characteristics

	number of drift cells	cell width (in.)	active area width (in.)	active area height	arm coordinate (from magnet) Z (in.)	arm coordinate (from magnet) Y
Fast pion-kaon arms						
0X	11	1	6	12	-255	0
0Y	11	2	6	12	-252	0
1X	8	2	9	16	-212	0
1Y	15	2	9	16	-209	0
2X	19	1	10	22	-93	0
2Y	39	2	10	22	-91	0
3X	11	2	12	38	80	0
3Y	37	2	14	38	85	0
3'Y	16	2	30	30	89.5	0
4Y	55	2	18	56	190	0
Slow pion arm (2 anodes/cell 1.5 mm apart)						
0U (D) Y	22	2.05		20.8	66.1	(-) 22.7
0U (D) X	20	2.05	18		69.9	(-) 22.7
1U (D) Y	28	2.05		26	89.4	(-) 29.0
1U (D) X	24	2.05	22.9		90.3	(-) 29.0
2U (D) X	28	2.05		26.3	112.5	(-) 34.9
2U (D) Y	34	2.05	34.9		113.5	(-) 34.9

Chapter V

THE PION BEAM

This experiment was mounted in the Fermilab High Intensity Area in the Proton West line. The buried beam line and experimental hall (Fig. 11) were designed to handle secondary beams of 5×10^{10} from 10^{13} primary protons on the target. All the magnets were conventional dipoles and quadrupoles with power supplies energized in synchronism with the main ring cycle.

The accelerator RF system caused protons extracted from the Fermilab main ring to arrive in 1 ns wide bunches every 18.6 ns. The negative secondary beam used by this experiment was produced by the primary proton beam striking a 1" square beryllium target 12" (one nuclear interaction length) long. The secondary particles were bent out of the target box by a 20° dipole that selected the desired charge secondary beam and dispersed the momentum components of that beam horizontally. After the magnet an 18° conical collimator with a 9.8 μsr aperture absorbed primary protons that had not interacted in the target, and also absorbed secondary particles with less than .6 of the central transmission momentum of the dipole-collimator combination.

PROTON WEST AREA

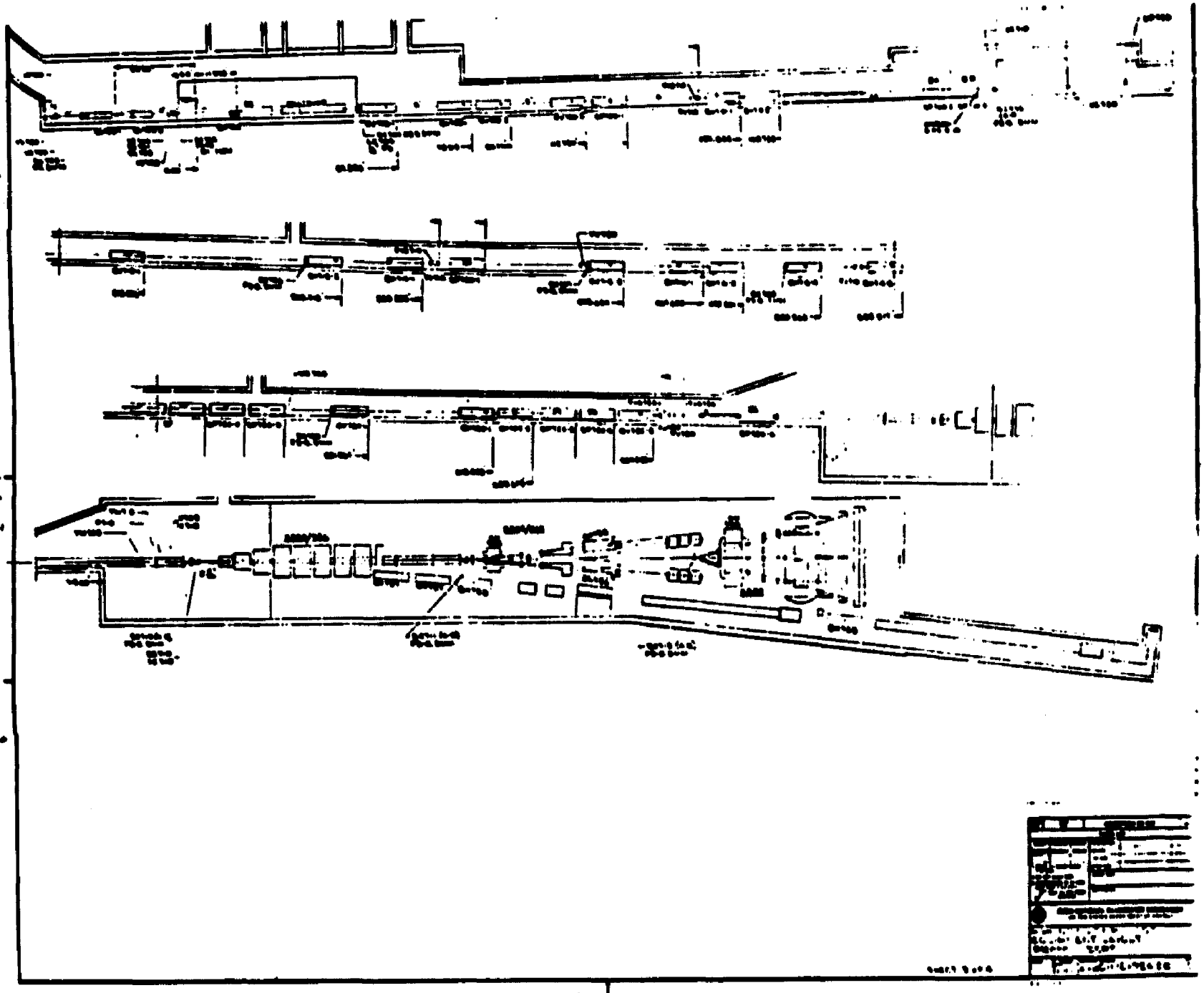

Figure 12

PION BEAM OPTICS

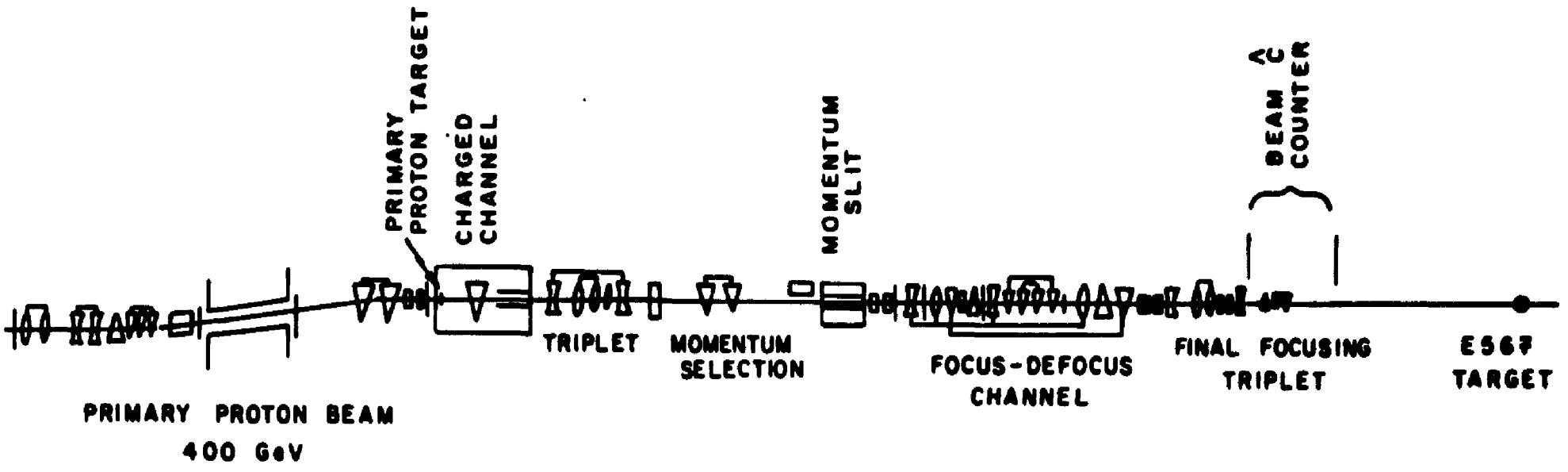

Figure 13

PION BEAM PROFILE

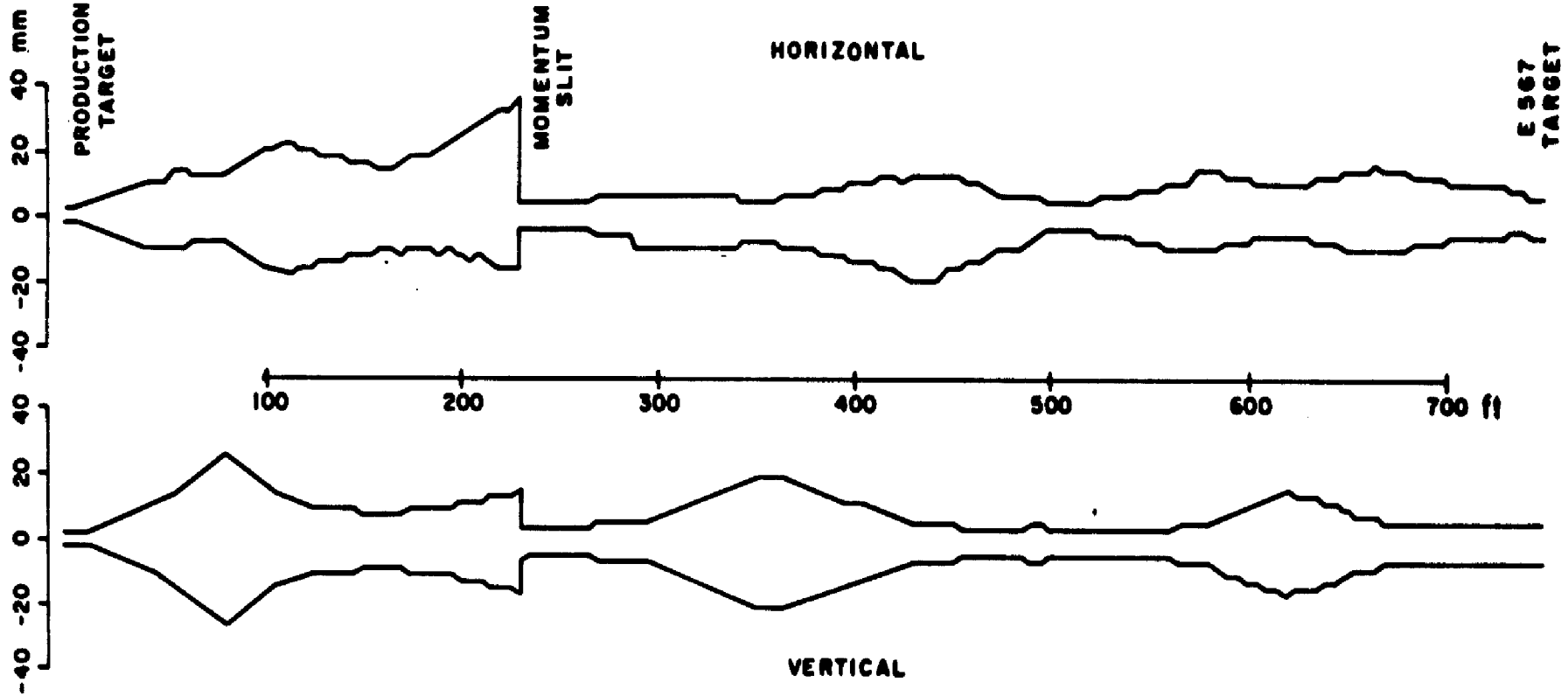

Figure 14

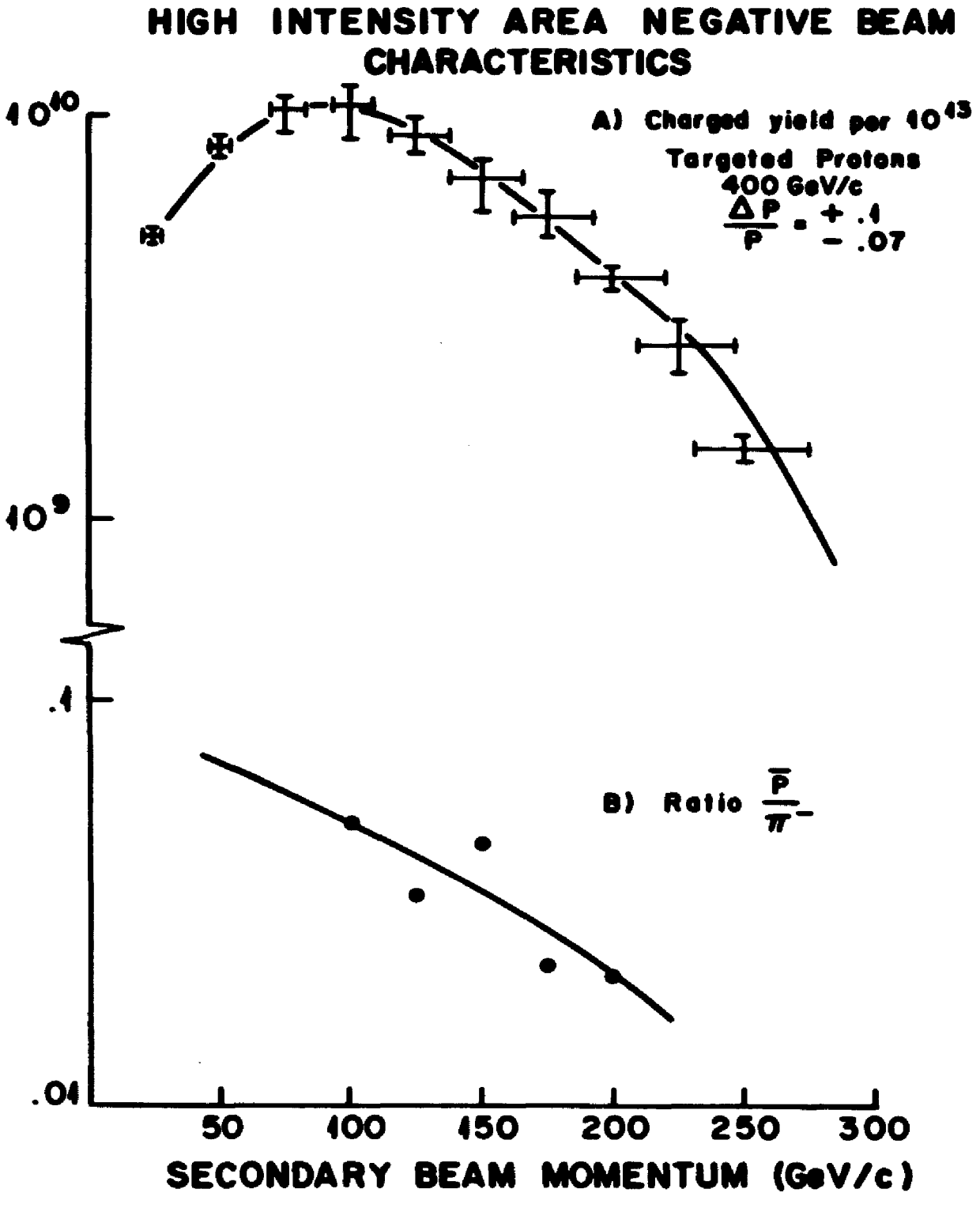
HIGH INTENSITY AREA NEGATIVE BEAM CHARACTERISTICS
4×10^{10}
10^9
.1
.01
A) Charged yield per 10^{13} Targeted Protons
400 GeV/c
$\frac{\Delta P}{P} = +.1 \; -.07$
B) Ratio $\frac{\bar{P}}{\pi^-}$
50
100
150
200
250
300
SECONDARY BEAM MOMENTUM (GeV/c)

Using the hadron production models of Bourquin and Gaillard (58) for the inclusive production of negative pions in p-p interactions, one gets $d\sigma/dpd\Omega\Big|_{p=100} = 38$ mb-sr^{-1}-GeV/c $^{-1}$ for 400 GeV/c incident protons. With the production target used this gives $dN/dpd\Omega\Big|_{p=100} = 1.3\times10^{14}$ sr^{-1}-GeV/c $^{-1}$ π^-'s per 10^{13} protons. At an angle of 0° the π^-:K$^-$:p production ratio is 20:6:1.

Fig. 12 shows the rest of the beam line, which was configured with a triplet and bend after the target box to focus the highly chromatic beam onto a 20' long adjustable horizontal collimator, the momentum slit, which passed particles in the selected range of momenta to the beam optics following it. These optics consisted of a triplet forming the front conjugate focus, a focusing-defocusing transport channel with a 3.4 mr bend for reducing decay muons from the beam, and finally a triplet for the final focus of the beam onto the experimental target. This quadrupole triplet was run asymmetrically to minimize the beam profile on the target. The beam spot measured at the target postion was routinely kept at less than 1" FWHM in both dimensions. Particle fluxes measured at the experimental hall by the beam counter are shown in Fig. 14. Since the beam Cerenkov counter was not used for identifying the incident beam particles during this experiment there was no restriction placed on the parallelism of the beam after the final triplet. Typi-

cal horizontal and vertical profiles from a computer model of the beam tune are shown in Fig. 13.

Segmented wire chambers were available at six locations in the line for monitoring the beam position. An ion chamber calibrated by foil activation was mounted immediately before the experimental target for integrating the total incident flux of charged particles. Trimming dipoles were available for correcting slight shifts caused by changes in the primary proton beam tune. The entire system, along with the power supplies for the spectrometer analyzing magnets was controlled and monitored by the Proton Area MAC computer system.

The acceptance bite, $\Delta P/P$, of the adjustable momentum slit was kept near the middle of the 1 - 10% range available. The slit aperture was varied as necessary with the proton beam intensity so sufficient pions impinged on the experimental target for triggering interactions to fill the data buffer. Generally 5×10^{11} protons per pulse were requested from the main ring to get 6.5×10^{7} pions per pulse at our experimental target. The secondary beam intensity was very sensitive to small shifts of the primary proton beam on the production target, requiring variations in the requested number of protons.

Toward the end of our data run large aperture, low current toroids were installed and powered in the P West beam line. These muon spoilers were designed to bend away from the detectors in the experimental hall muons originating from decays of secondary beam particles that formed a halo about the beam pipe. They decreased the singles rates in the muon counters by a factor of 13 but had no significant effect on this experiment.

Chapter VI

TRIGGER AND DATA COLLECTION

In setting up the fast trigger logic all scintillation counter voltages were adjusted to give a 120 mV output into 50Ω for minimum ionizing particles, and then pulse arrival times matched to within one ns for elements within a given hodoscope. The signal from each PM tube was split 10:1, with the high output discriminated at 50 mV in stock LeCroy octal and quad discriminator units set to give 10 ns wide NIM logic signals. The low level output from the passive splitter went to a 4:1 linear fan-in and then a 10x amplifier for input to the pulse height monitoring ADC.

Threshold and differential Cerenkov counter PM tube voltages were set to give a single photoelectron peak at 20 mV. These PM outputs also went through 10:1 passive splitters with the outputs from the two tubes in a threshold counter going to a linear fan-in, the output of which was discriminated at a 30 mV level to give a trigger logic signal and the low level sent to the ADC's after a 10x amplification. The differential counter information was not used in the trigger logic, so the high level output from the splitter

was sent directly to an ADC and the low level amplified and then discriminated to give a logic signal for setting a pattern bit.

Standard NIM logic units were used to define the following logic conditions from the Cerenkov and hodoscope discriminator outputs (all right arm and down signals mirrored left and up):

$$\text{LEFT} = \sum_i \text{FIL}_i \bullet \sum_i \text{BOL}_i \bullet \sum_i \text{BIL}_i \bullet \sum_i \text{BIIL}_i$$

$$\text{UP} = \sum_i (\text{UPT})_i \bullet (\text{UPIT})_i$$

TC = Threshold Counter

$$\mu_L = \Sigma(\mu\text{IL} + \mu\text{IIL} + \mu\text{IIIL}) > 1$$

$$\text{HS} = \text{UP} + \text{DOWN}$$

$$\text{L}\bullet\text{R} = \text{LEFT}\bullet\text{RIGHT} .$$

Coincidences between specified counters in BIY and BIIY hodoscopes gave bending angle information which indicated a particle's charge and also allowed a crude momentum determination that could be used in the fast trigger. Two 10x10 fast coincidence arrays for each fast arm were employed to define the logic signals $P_{L^+R^-}$ and $P_{L^-R^+}$. Monte Carlo studies determined which coincidences were desired to select particles with $p > 5$ GeV/c.

Using these logic variables the data triggers for the experiment could be implemented:

$$D^* = (L\bullet R)\bullet\overline{(TC_L \bullet TC_R)}\bullet\{\text{UP}\bullet(P_{L^-R^+}\bullet TC_R + P_{L^+R^-}\bullet TC_L) + \text{DOWN}\bullet(P_{L^-R^+}\bullet TC_L + P_{L^+R^-}\bullet TC_R)\}\bullet\text{HS}\bullet(TC_L + TC_R)$$

$$\mu = (L\bullet R)\bullet(\mu_L\bullet\mu_R) .$$

Figure 15

E567 MAIN TRIGGER
(ONLY UP AND LEFT ARMS SHOWN)

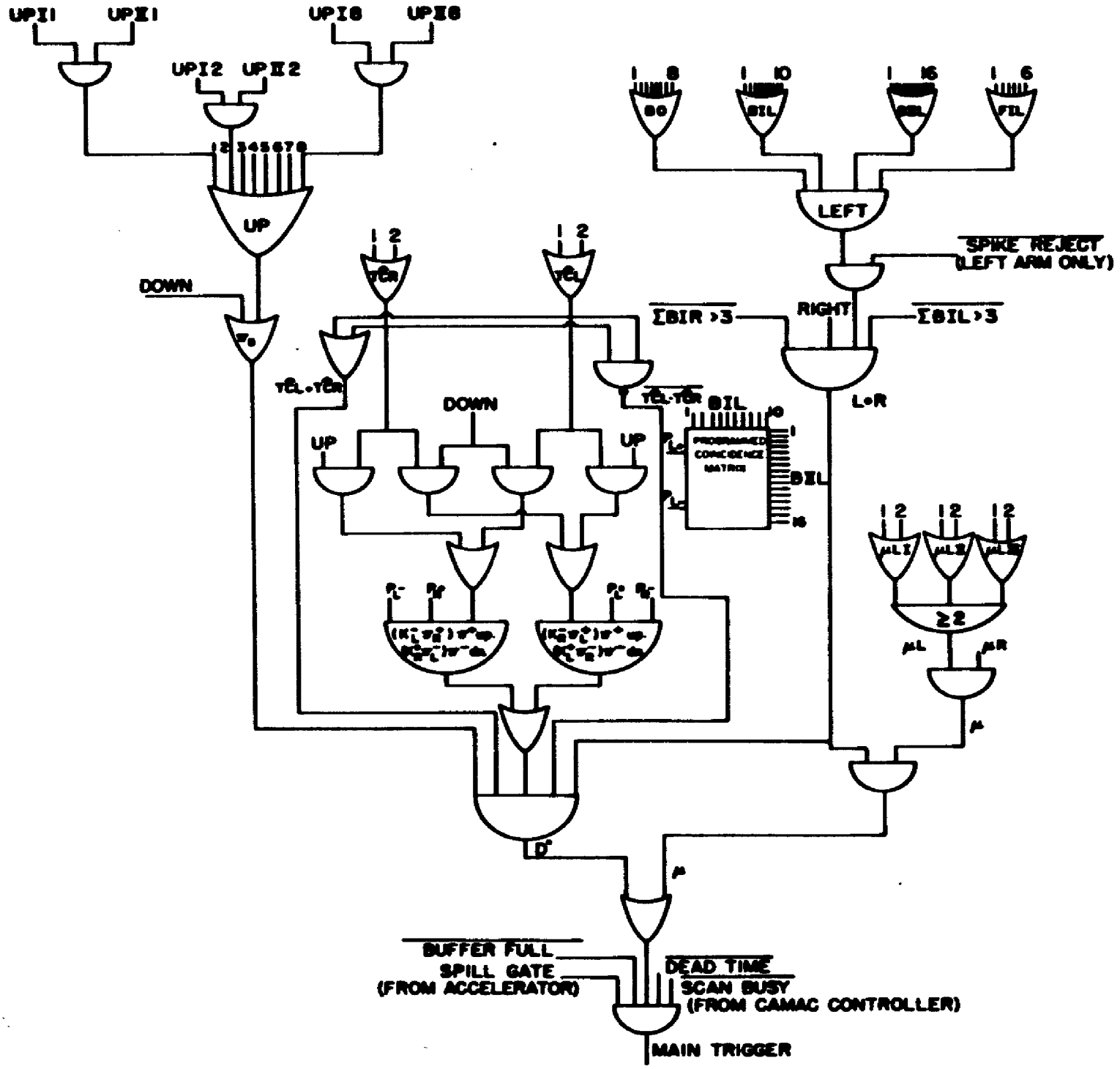

These are shown schematically in Fig. 15 . The D* trigger shown was used for a majority of the data. It selected events that could be the expected decay modes of the charged D*'s: $[K^+\pi^-]\pi^-$ and $[K^-\pi^+]\pi^+$, where the bracketed particles are those analyzed in the two fast arms. A trigger that required an oppositely charged $[K\pi]$ and a particle of either sign in the slow arm was used for 12% of the data analyzed. Less restrictive triggers were used as required for system checkout and alignment data. Most of the logic variables were continuously scaled so trigger efficiencies could be monitored from run to run and any problems with the apparatus and or trigger logic quickly recognized. A scaler readout for a sample run is shown in Table 4. Quantities are normalized by the incident flux measured in the ion chamber located at the target.

TABLE 4

RUN 382 Scalers

D* triggers	.055
$\mu \cdot \mu$	.064
ns	758
L•R	1.8
$P_{L^+R^-}$	.37
$P_{L^-R^+}$	.24

(per 10^5 pions incident)

Studies of trigger rates and reconstruction efficiencies showed that the experimental apparatus was swamped by high instantaneous beam fluxes, and was subject to high multiplicity splashes in the hodoscopes and chambers behind the fast arm analyzing magnets. These problems were ameliorated by using the output of the beam Cerenkov counter, discriminated at a level corresponding to five particles in a RF bunch, to veto the trigger signal. A multiplicity greater than two in either PII hodoscope would also veto the signal for that arm.

The status of all logic signals, counter timing and pulse heights, wire drift times from the chambers, scalers, and fixed run information were logged for each event by a CAMAC based data acquisition system. Triggers from the fast logic system within the spill gate set by accelerator timing signals and the readout system dead time gate initiated a scan of the CAMAC system into the buffer memory. The trigger was also the stop signal for the CAMAC TDC's, the drift chamber timing system, and the sampling gate for the CAMAC ADC channels and logic pattern words. All data inputs to the CAMAC system except for the drift chamber signals were delayed by 132 ns with coaxial cable to allow for signal propagation time through the trigger logic. Chamber stop signals were timed in separately for each of the nine readout modules.

TABLE 5

CAMAC Event Format

Data	Words
Fixed run data	4
Pattern words	11
TDC's	72
ADC's	72
Scalers	24
Drift chamber time digitizers	9 - 905, 200 average

Approximately 2 ms were required to readout the 350 - 450 16 bit words in an event leading to deadtime losses of 15 - 30%, depending on the spill length and quality of the delivered beam. The number of events stored in the memory each spill varied between 36 - 48 depending on the number of drift wires active in the events, which was a function of the instantaneous intensities encountered. Data were accumulated during periods of half second and one second spills from the accelerator. Some 40% fewer extraneous chamber and counter hits were recorded in data taken during one second spill operation.

For maximum reliability and flexibility no on-line filtering or compression of data was done. All information from the CAMAC data logging system was stored in a buffer

memory and subsequently written to tape. The buffer size limited the number of events that were desired in a spill. Under the optimum conditions of one second spill and stable beam intensity, an event rate three times as great could have been accepted without degrading track reconstruction capability. Since a large amount of the data was taken under adverse conditions this limitation on the number of triggers per pulse that could be recorded was not a severe restriction. By using a data acquisition system independent of a computer we were not dependent on hardware and software relability and also had an independent backup if the primary tape system failed. Fortunately, this redundancy was not required since the system was reliable. One tape drive malfunction caused the loss of data accumulated for approximately half a day.

The 16Kx16 bit core memory was dumped onto 9 track, 800 bpi tape in four 8K tape character records when all 16K were full or at the end of the spill. An HP2116B computer monitored the first 4K words of each spill written into the buffer and accumulated performance data on all of the over 1000 signals available from the apparatus and logic. In addition it performed system functions such as CAMAC system resets and maintaining scaler information. The information flow in the data acquisition system is shown in Fig. 16.

Figure 16

E567 DATA ACQUISITION SYSTEM

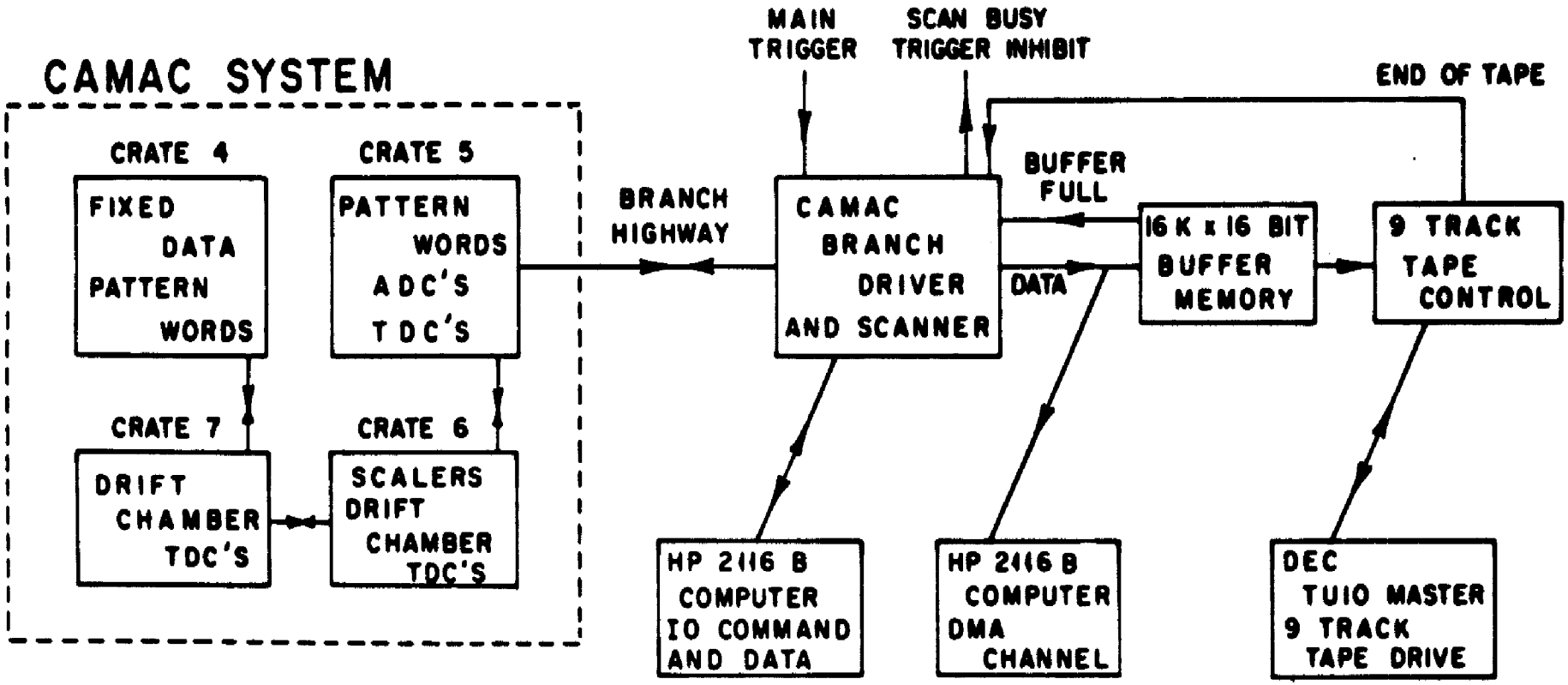

The commercially built drift chamber time digitizers turned out to be the most troublesome pieces of equipment in the system. These were designed to digitize, with eight binary digits precision, the time between separate channel start signals from the drift chamber amplifiers and a common stop signal from the trigger logic. The module complemented these eight bits to give the drift time vs. distance relationship, and put the channel number in the high order eight bits of the sixteen bit data word. The packing density of 96 digitizers in a triple width CAMAC module was far too high. The power requirements for each module necessitated the use of external power leads and careful ventilation. Another contributor to the unreliable behavior of these nine units was the serial readout of all the channels within a TDC module in one chain, allowing one bad channel to block the information from all those following it.

The modules were initially adjusted to give approximately 3.3 ns per count. Each channel was individually calibrated eventually because of channel to channel variations within a module. There were slow drifts with time in many modules' calibration and one module was subject to major erratic shifts within short time spans. Fortunately the two plane, staggered cell design used in the fast arm chambers constrained the sum of drift times for events with hits in both planes and allowed these shifts to be detected and corrected in off-line analysis.

ADC and TDC pedestals were determined from tapes written with a pulser trigger at roughly ten day intervals. Correction sets derived from these tapes were applied to the counter data in off-line analysis.

Chapter VII

TRACK RECONSTRUCTION AND DATA ANALYSIS

Initial and secondary analysis of the data were carried out on the Fermilab CYBER 175 computer system. A D* event with a track found in each spectrometer arm or a muon event with tracks in the two fast arms was written onto high density secondary tapes for further analysis. Event data saved included ADC and TDC readouts with pedestals subtracted, pattern words, scalers, and the coordinates of chamber points for the reconstructed tracks. Processed data, such as expected scintillation counter timing, were also recorded.

The reconstruction routine for fast spectrometer arm tracks was developed and tested in the analysis of Brookhaven AGS Experiment 604 with the intent of utilizing it for the analysis of the primary data tapes in this experiment also. The program started by defining roads that could contain a track using the scintillation counter position information and the target. If a track was detected in only one plane of a drift chamber a point was defined, and if both planes in a chamber registered hits, a line through them was defined. The track finding process was controlled by 34 vectors determining the order in which chambers were

searched for points and lines that lay within the roads capable of forming line segments between chambers. As information on a possible track was accumulated roads through chambers not yet searched were narrowed. Success or failure in finding acceptable points in the chamber pair being searched indicated the direction of the vector to the next pair to be searched. As experience was gained with the track finding process, the program flow was readily changed by changing the pointers in the flow vectors, insuring the most likely searches were conducted first and eliminating searches that were usually futile.

The program started track reconstruction with the Y view line segment after the BM109 analyzing magnet. If successful, it constructed a road between the target and the segment intercept at the center of the BM109, and a line segment through the three chambers in the front of the arm was searched for hits to reconstruct the entire track Y view. After finding the Y view of a track the program would attempt to find the X view, which was somewhat simpler since there was no bend point to prevent a straight road from being constructed between the target and the Y hodoscope close to the last X viewing chamber. Up to two separate tracks in each fast arm could be reconstructed. The hodoscope tilted at 26.5° was used to match X and Y views when more than one track was reconstructed in an arm.

The tracks in the slow spectrometer arm were found in an analogous manner, although there was no information about these tracks' positions before the magnet in that arm. First pass analysis assumed a straight line segment through the center of the target and the center of the magnet that joined with a line segment found through the Y view chambers. Roads for the Y view were formed by the collimator aperture and the trigger counter pairs, but the only constraints for line segments in the X view came from the magnet aperture (±100 mrad) and the intercept at the target plane (± 8.5 cm.). X and Y views of reconstructed tracks were required to be within .45 cm. of each other in the middle X viewing chamber in which the wires were at a 7° stereo angle. This meant that any track in the X view that contained only two chamber points had to have one of them in the central chamber. A track in this arm had to have at least five points to be considered successfully reconstructed. Up to four tracks in a single event could be reconstructed in this arm, two for each particle polarity.

The track finding progam was tested with tapes written using simple apparatus triggers and the analyzing magnets off. The usual target positioned 60.1" in front of Henry Higgin's center was replaced by a 1 cm. aluminum cube at the center of that magnet for aligning the slow arm. Individual sense wire positions were determined using these straight through tracks.

Track finding efficiency was excellent for the fast arms, averaging 75% for tracks that warranted a full attempt at reconstruction by satisfying some crude momentum and vertex conditions. Reconstruction efficiency for the slow arm, at 70%, was somewhat less because of the fewer chamber planes available.

All subsequent analysis was carried out with the secondary tapes generated by the track finding program. An average of 8000 reconstructed events were written onto a secondary file from each primary run tape. In analyzing the data it was seen that Λ, $\bar{\Lambda}$ and $\phi(1020)$ peaks could be observed in the $p\pi$ and single arm K^+K^- particle mass spectra (Figs. 17,18), and tapes were generated of events that met the selection criteria for these particles in addition to the tapes that contained the D* and di-muon events. Three generations of D* tapes were generated from the secondary tapes. The tertiary tapes contained 555 thousand events with identified $K\pi\pi$ system tracks satisfying a target vertex requirement that rejected 42% of the events. The quaternary tapes held 131 thousand $K\pi\pi$ events from the tertiaries with the additional cut: $M(K\pi\pi) - M(K\pi) - M(\pi) < 25$ MeV/c^2. The final sample consisted of 26 thousand events with $2 < M(K\pi\pi) - M(K\pi) - M(\pi) < 9$ MeV/c^2. After this last file was generated a test was made on approximately 30% of the data on the secondary tapes to insure that corrections to the analysis

Figure 17

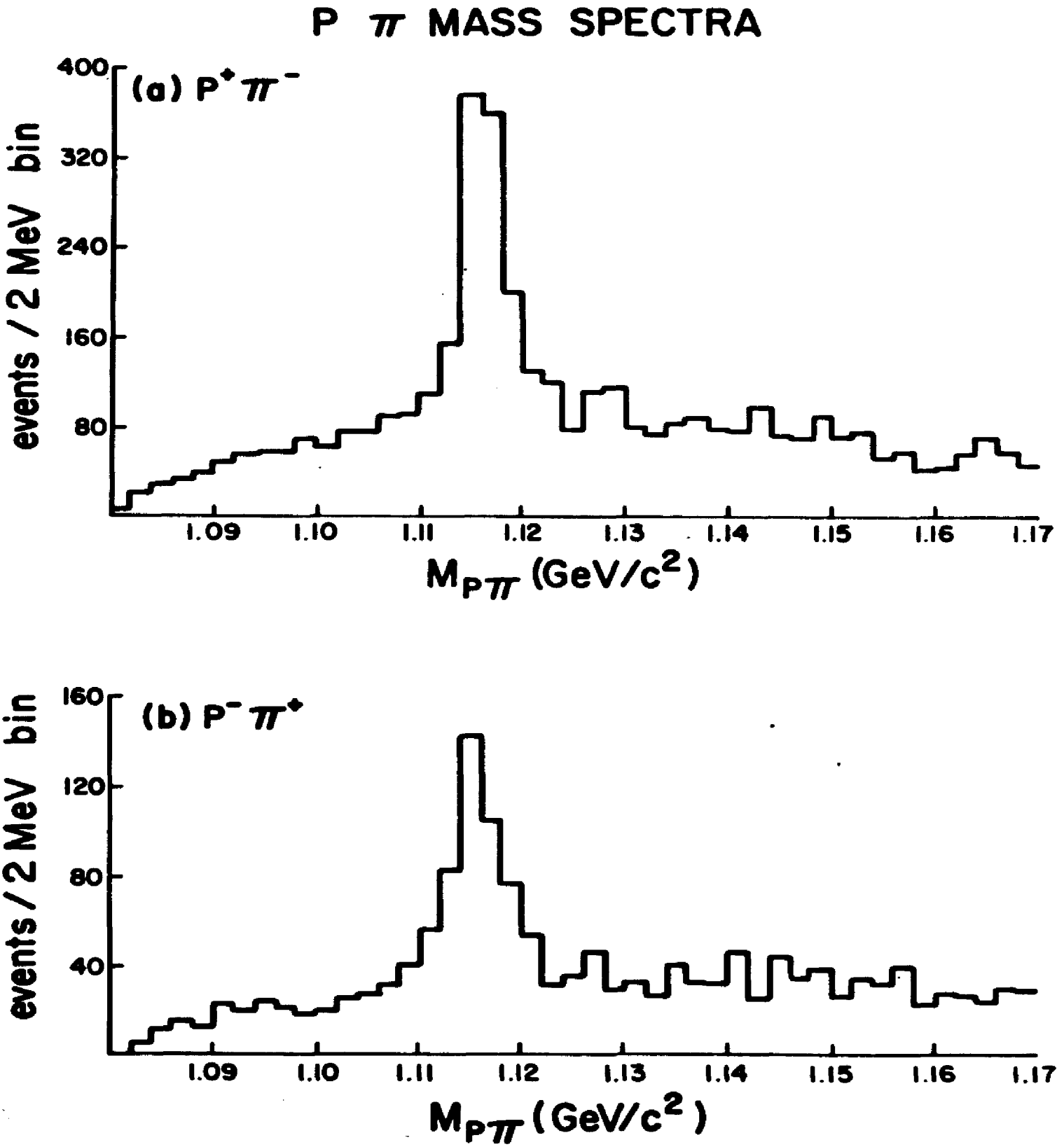
P π MASS SPECTRA
(a) P⁺π⁻
events / 2 MeV bin
400
320
240
160
80
1.09
1.10
1.11
1.12
1.13
1.14
1.15
1.16
1.17
M_Pπ (GeV/c²)
(b) P⁻π⁺
events / 2 MeV bin
160
120
80
40
1.09
1.10
1.11
1.12
1.13
1.14
1.15
1.16
1.17
M_Pπ (GeV/c²)

Figure 18

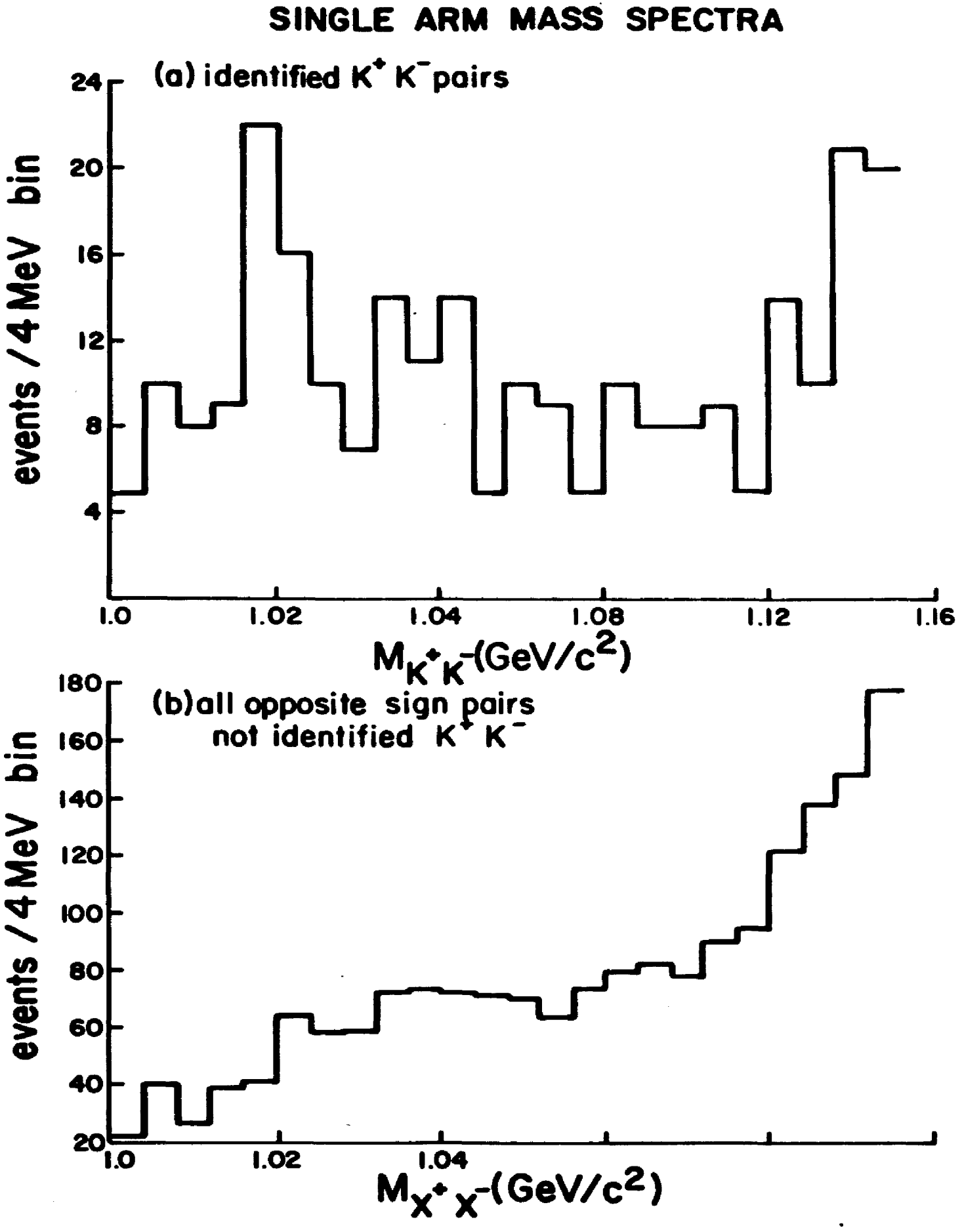
SINGLE ARM MASS SPECTRA
(a) identified K⁺ K⁻ pairs
events /4 MeV bin
24
20
16
12
8
4
1.0
1.02
1.04
1.08
1.12
1.16
M K⁺K⁻ (GeV/c²)
(b) all opposite sign pairs
not identified K⁺ K⁻
events /4 MeV bin
180
160
140
120
100
80
60
40
20
1.0
1.02
1.04
M X⁺X⁻ (GeV/c²)

added after the tertiary tapes were written did not substantially effect the results. Less than a one percent change in the events per bin was noted in the K_{π} mass spectra from the primary runs in this test data compared with the same primary runs in the final sample. Hence, no effort was made to re-analyze all the secondary tapes.

Observation of the J/ψ peak in the opposite charge dimuon mass spectrum (Fig. 19a), gave us confidence that the two fast arms were working correctly. The Λ and $\bar{\Lambda}$ peaks seen in the mass spectra obtained from a fast arm proton and a slow arm pion (Fig. 17) showed the fast arms and slow arm were properly coordinated. In addition, these p_{π} peaks were useful for detecting any systematic differences in momentum calibrations between the two fast arms and the the two sections of the slow pion arm, UP (positive) and DOWN (negative), since the Y vertex position of the fast particle was used to determine the slow arm track slope before the analyzing magnet.

The $\mu^+\mu^-$, p_{π}, K^+K^-, mass spectra also allowed a determination of the four magnetic field parameters: the three magnet $P_{\perp}$'s and the offset of the magnetic bending center from the pole piece center in Henry Higgins. The sum of the two BM109 $P_{\perp}$'s was set by requiring the correct J/ψ mass, since this was sensitive to the average of the muons' momenta, and

Figure 19

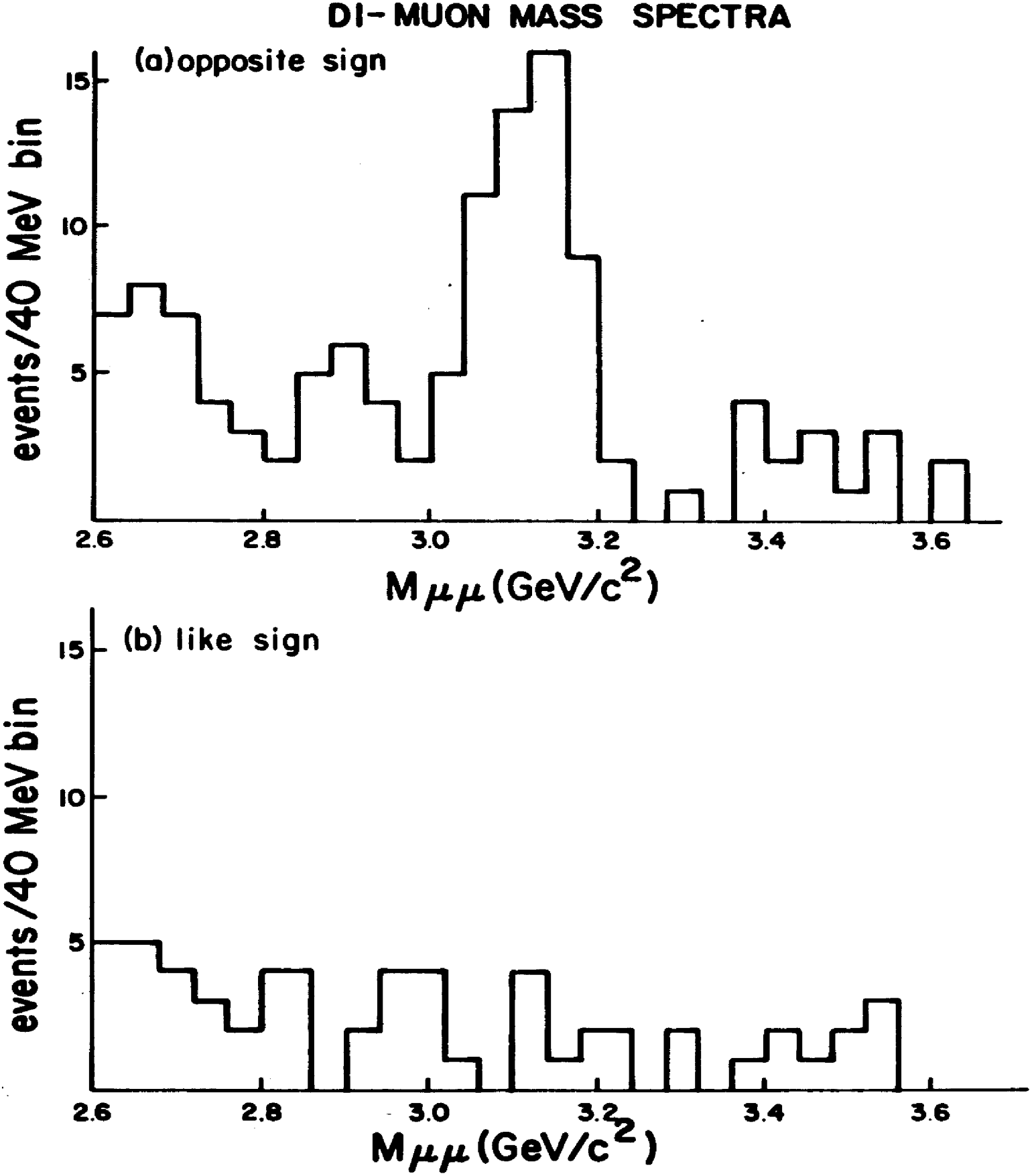
DI-MUON MASS SPECTRA
(a)opposite sign
events/40 MeV bin
15
10
5
2.6
2.8
3.0
3.2
3.4
3.6
Mμμ(GeV/c²)
(b) like sign
events/40 MeV bin
15
10
5
2.6
2.8
3.0
3.2
3.4
3.6
Mμμ(GeV/c²)

the fast arm momentum was directly proportional to the $P_\perp$ in that arm. When analyzing events with two tracks reconstructed in an arm, a ϕ peak could be seen in the di-kaon spectrum available from both fast arms. Since $M_\phi \cong \sqrt{P_1 P_2}\ \theta$, with the opening angle θ of the kaons determined by Henry Higgins' $P_\perp$ and $P_\parallel$, P_2 linearly dependent on the BM109 value in that arm, fixing the two arm average ϕ peak gave a value for Henry Higgins' $P_\perp$. Requiring the two arms give the same ϕ mass fixed the deviations from the average of the two BM109 values.

With the $P_\perp$'s fixed by this procedure the shift in the magnetic center of Henry Higgins was then determined to be 1.3" upstream of the physical center by requiring that the vertex of all two track events coincide with the target. Later studies have included information obtained from a field map made with a hand held Hall probe, and have shown that the offset depends on the horizontal position of a track at the magnet's exit. The offset value was changed to 1.25" for tracks within the geometric acceptance of the slow pion spectrometer.

Chapter VIII

ANALYSIS RESULTS AND CONCLUSIONS

This experiment was designed to be sensitive to the decay sequence: $D^{*+} \rightarrow D^0\pi^+$, $D^0 \rightarrow K^-\pi^+$, and its charge conjugate. The invariant quantities we chose to examine for the signature of these decays were the $K\pi$ mass in the two fast arms and the difference between the $K\pi\pi$ system mass and the sum of the $K\pi$ mass and well known π mass. The second quantity is the Q-value for the $D^* \rightarrow K\pi\pi$ reaction. These two variables were independent of each other. Other possibilities such as the three body $K\pi\pi$ invariant mass and the slow pion momentum in the c.m. frame of the $K\pi\pi$ system were investigated, but no advantage was seen in using them. Histograms and scatterplots were fit using the maximum likelihood method and assuming a Poisson distribution of the observed number of events in a histogram bin about the true value described by the background and peak functions. The CERN computer library program MINUIT was utilized for the maximization.

Functions describing the backgrounds were investigated in several manners. Monte Carlo programs were used to generate $K\pi$ mass and $[K\pi]\pi$ Q-value distributions using the particle

distributions observed in this experiment or inclusive differential cross sections measured in other experiments. Tracks from different events were combined and then analyzed as if real events. Q-value distributions were made from events with the wrong sign slow pion for D* decay, ie. $[K^+\pi^-]\pi^+$. Consistent values for the coefficients of a polynomial form for the $K\pi$ mass background, $A\{1 + B(M_{K\pi} - 1.85) + C(M_{K\pi} - 1.85)^3\}$, and an exponential form, $D(1 + EQ)(1 - \exp(-.5Q \cdot ^7))$ for the Q-value background were obtained from these methods. The histograms obtained from the final data sample of correct sign $K\pi\pi$ events were fitted to these background forms plus a Gaussian peak having a width corresponding to the apparatus resolution of the variable being fit: 14 MeV for $K\pi$ mass peak and .6 MeV for the peak in Q-value.

As seen in Figs. 20 and 21 the $K\pi$ mass spectrum and the Q-value distribution without imposing cuts on the data based on $D^* \rightarrow D\pi$ measurements are smooth, with no peaks indicating particle production. It was necesary to make cuts on the data sample using charmed particle mass measurements made at SPEAR.

Separate fitting procedures to three distributions were carried out, summing $K^+\pi^-\pi^-$ and $K^-\pi^+\pi^+$ events. The background and peak fits for the Q-values with $1.835 < M(K\pi)$

Figure 20

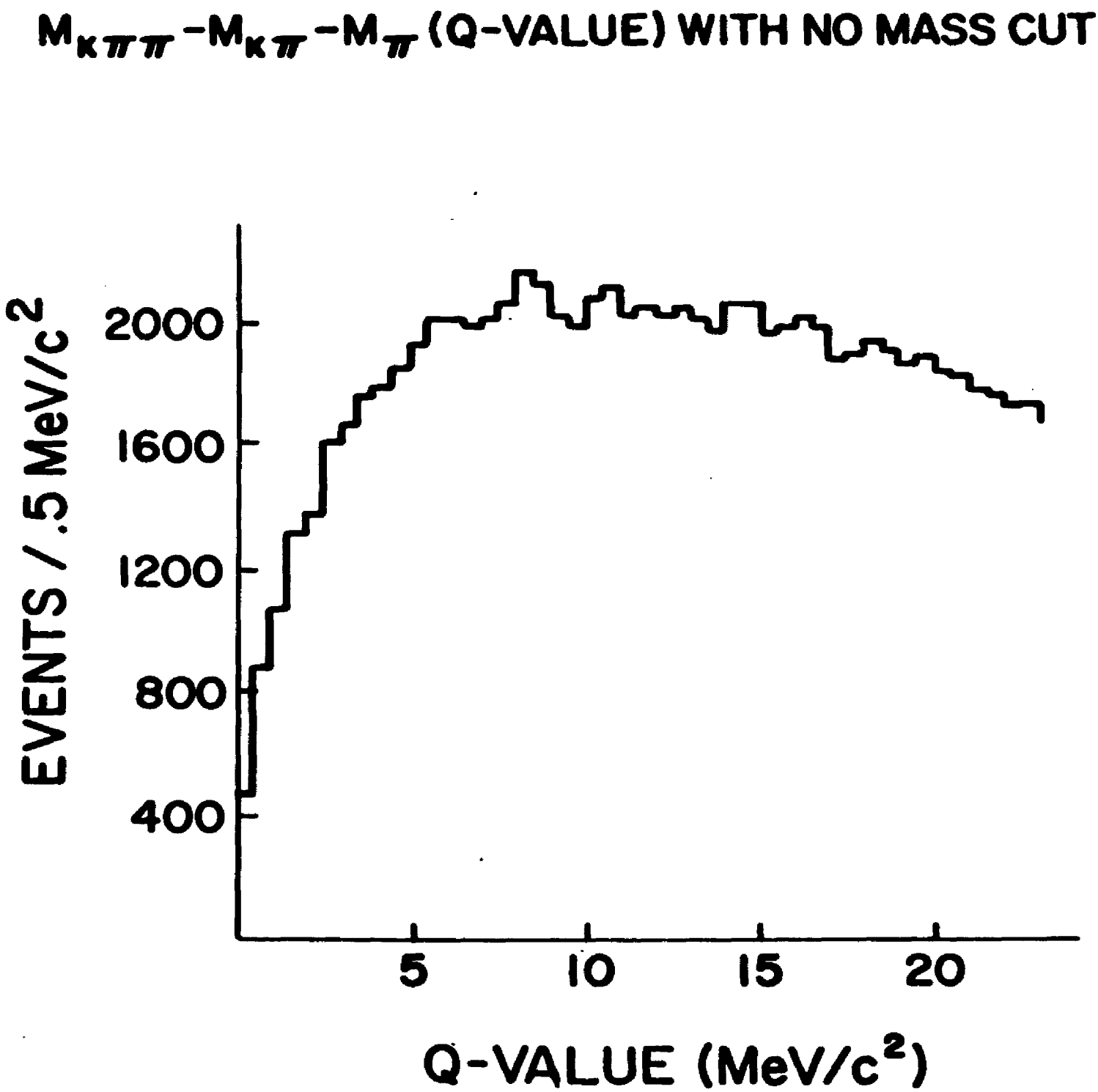
$M_{K\pi\pi} - M_{K\pi} - M_{\pi}$ (Q-VALUE) WITH NO MASS CUT
EVENTS / .5 MeV/c^2
2000
1600
1200
800
400
5
10
15
20
Q-VALUE (MeV/c^2)

Figure 21

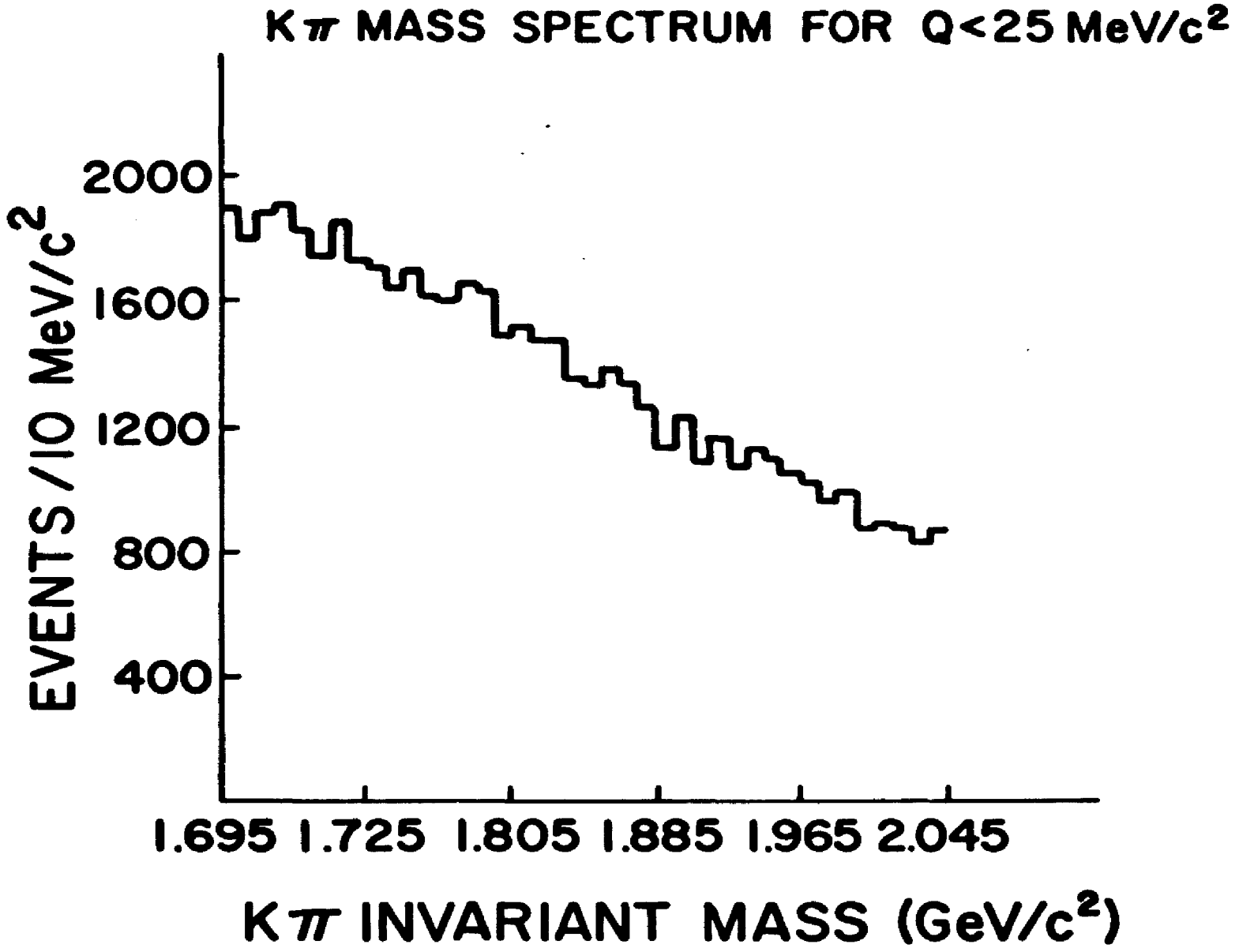
Kπ MASS SPECTRUM FOR Q<25 MeV/c²
EVENTS/10 MeV/c²
2000
1600
1200
800
400
1.695 1.725 1.805 1.885 1.965 2.045
Kπ INVARIANT MASS (GeV/c²)

Figure 22

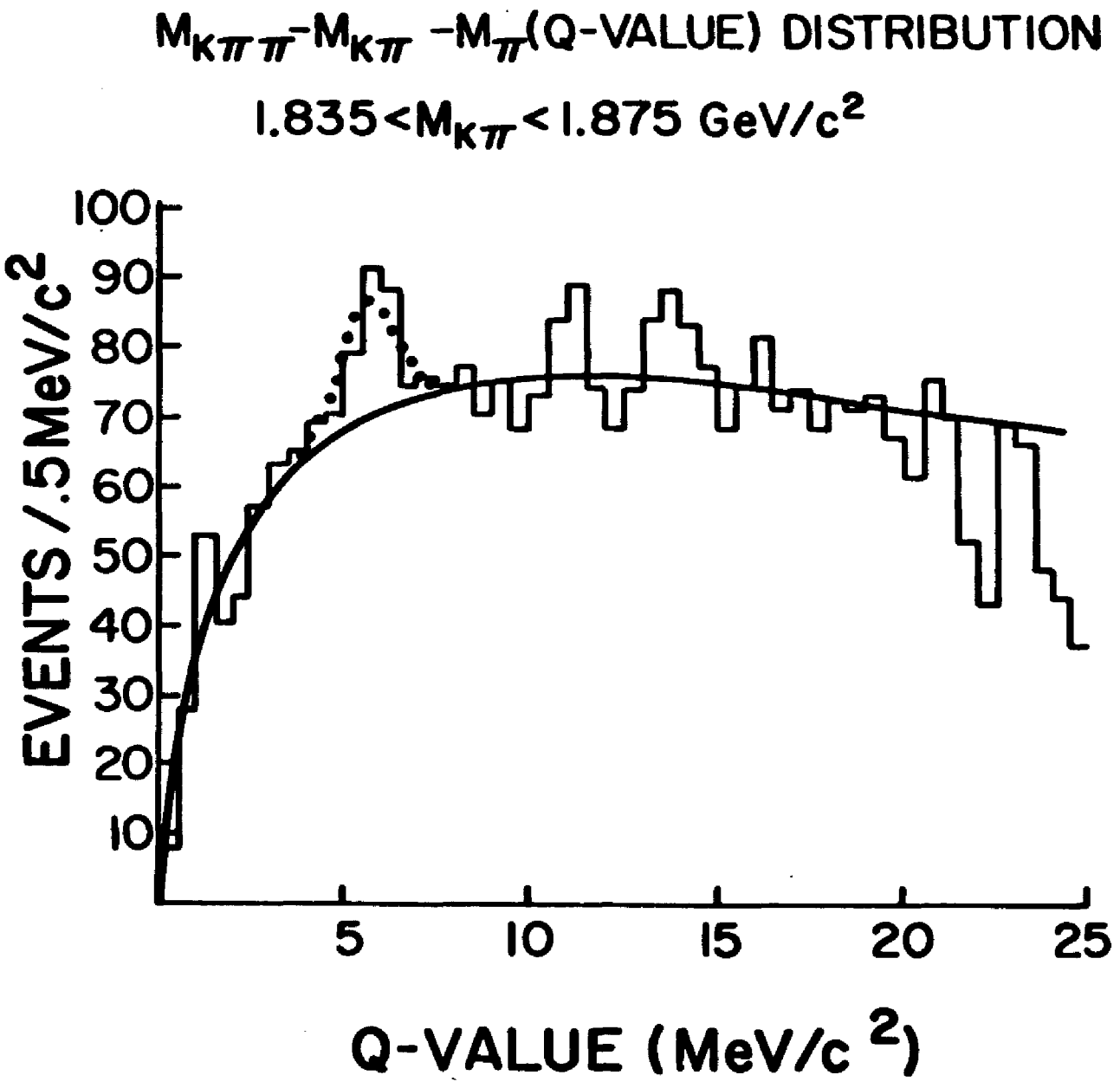
$M_{K\pi\pi}-M_{K\pi}-M_{\pi}$(Q-VALUE) DISTRIBUTION
$1.835<M_{K\pi}<1.875$ GeV/c^2
EVENTS/.5MeV/c^2
100
90
80
70
60
50
40
30
20
10
5
10
15
20
25
Q-VALUE (MeV/c^2)

Figure 23

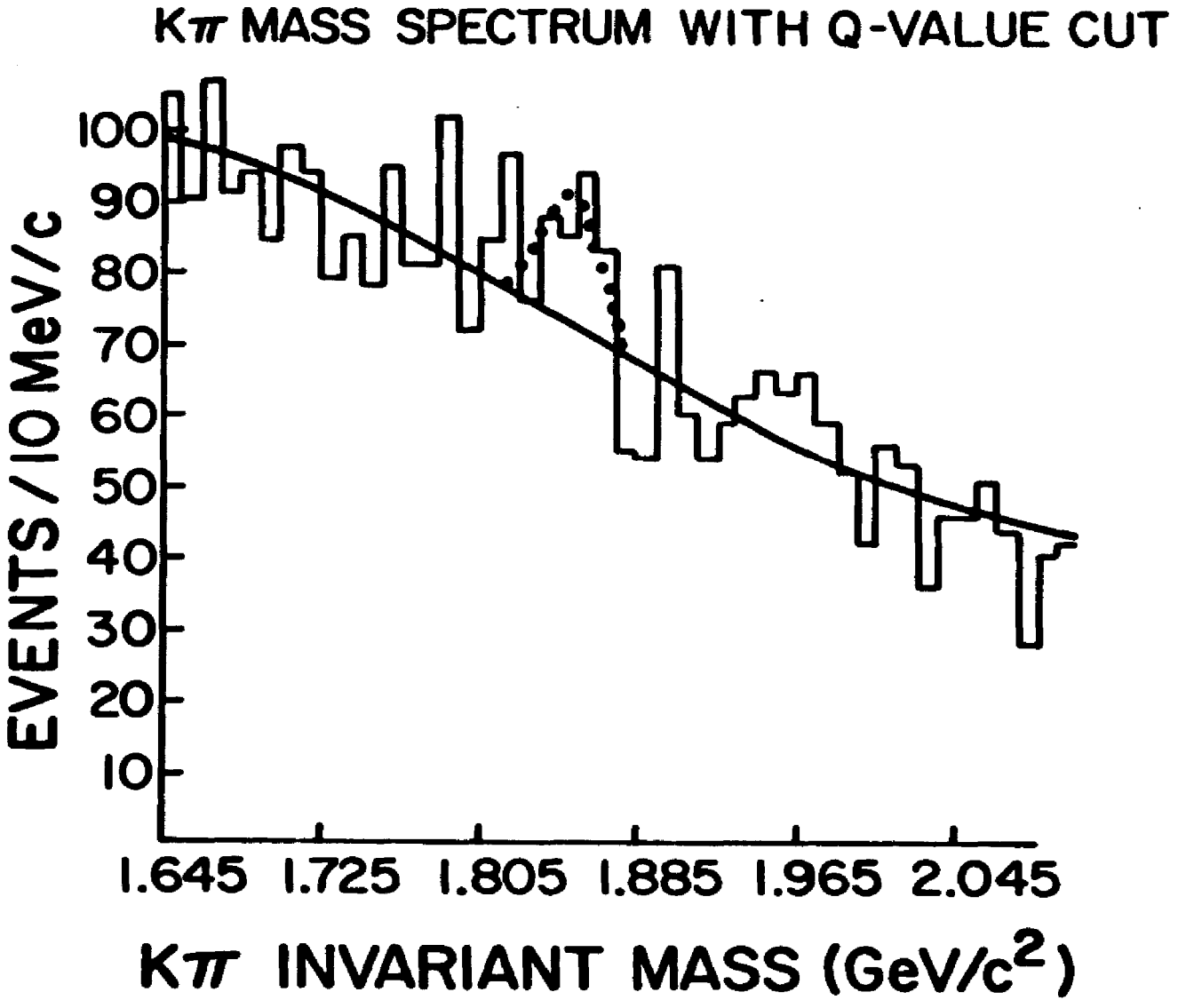
Kπ MASS SPECTRUM WITH Q-VALUE CUT
EVENTS / 10 MeV/c
100
90
80
70
60
50
40
30
20
10
1.645
1.725
1.805
1.885
1.965
2.045
Kπ INVARIANT MASS (GeV/c²)

<1.875 GeV/c^2 are shown in Fig. 22, while the D^0 mass with a cut on Q-value based on the expected resolution δ of this variable is shown in Fig. 23. The kinematic dependence of the Q-value resolution δ is discussed in Appendix II. In addition, a two dimensional Gaussian peak was fit to the scatterplot of Q-value vs. M($K\pi$), using a background form that was the simple product of the individual backgrounds in the M($K\pi$) and Q-value distributions. The results of these fits are shown Table 6. These three distributions all give a consistent number of D* events reconstructed from the data.

These results are readily converted into a cross section measurement using the J/ψ peak in the opposite sign di-muon mass spectrum to determine the flux normalization. The $\pi^-N \rightarrow \mu^+\mu^-$ differential cross section has been measured at $\sqrt{s}$ = 20.5 GeV in a wide acceptance di-muon experiment at Fermilab (59). Interpolating on the $pN \rightarrow J/\psi + X$ excitation curve (60), a reduction of 12% in this cross section at the $\sqrt{s}$ = 19.4 this experiment was conducted at is assumed, giving $F d\sigma/dx\Big|_{x=0} = .062$ μb-GeV-(unit x)$^{-1}$.

Since the D* acceptance of the apparatus is sharply peaked at x=.03 the data was analyzed to give a differential cross section $d\sigma/dx$ to minimize the production model dependence. This measurement still depends on the P_T dis-

TABLE 6

Peak Fits

	Q-value	M	Q vs M scatterplot
peak values (MeV)	5.8±.3	1854±6	
cut values (MeV/c^2)	5.9±1.3σ	1855±20	
peak width (MeV/c^2)	.7	14	.6, 14
χ^2/dof for fit	.66	1.17	1.02
# background events	413±46	365±11	
peak significance	3.0σ	3.3σ	2.3σ
# events in fitted peak	63±21	70±21	53±23
# events without cut	74±25	85±25	

tribution assumed in the model. The narrow x region accepted by the fast spectrometer arms allowed the approximation:

$$\int A(x)\, d\sigma/dx\, dx \sim d\sigma/dx\Big|_{A_{max}} \int A(x)dx \sim d\sigma/dx\Big|_{A_{max}} \langle A\rangle \Delta x \ .$$

When determining the total acceptance, $\int A(x)dx$, Monte Carlo events were generated with a production distribution $dN/dx = (1-|x|)^b$. The dependence of acceptance on the exponent b was removed by defining

$$\Delta x\langle A\rangle = \frac{\int dN/dx\, dx}{dN/dx} \int A(x)\, dx \ .$$

For J/ψ inclusive production b was taken to be 1.65 from the fits to the di-muon data in reference (59); at the peak acceptance point $x=.07$, $\Delta x\langle A(\psi)\rangle=8.2\times10^{-4}$; D* acceptance peaked at $x=.03$, and assuming $b=3$, $\Delta x\langle A(D^*)\rangle=1.9\times10^{-4}$.

Trigger and analysis losses for D* and J/ψ detected by the spectrometer system are summarized in Table 7. These fractional losses were assigned either from Monte Carlo simulation (kaon decay within a spectrometer arm or momentum matrix cut) or from primary and secondary analysis statistics.

TABLE 7

Detection and Recovery Efficiencies

	$\mu^+\mu^-$	D*
Track reconstruction	$(.75)^2$	$(.75)^2(.7)$
Right-left vertex cut	.7	.7
Slow pion vertex cut		.9
Trigger hodoscopes	$(.99)^8(.94)^2$	$(.99)^8$
K decay in fast arm		.82
Momentum matrix acceptance	----	.91
Overall efficiency	.32	.18

Since the cross section equals:

{(# events)}/{(flux)(acceptance)(efficiency)(Branching Ratio)}

and recalling that the D* data was summed over the two charge states one finds for $\pi N \rightarrow D^{*+} + X$:

$$\frac{d\sigma}{dx} = \frac{(.5)(\#\ D^*\ \text{events})(J/\psi\ \text{efficiency})\langle A(\psi)\rangle d\sigma(\pi N \rightarrow J/\psi + X)/dx}{(\#\ \mu^+\mu^-\ \text{events})(D^*\ \text{efficiency})\langle A(D^*)\rangle BR(D^* \rightarrow D\pi)\, BR(D \rightarrow K\pi)}.$$

SPEAR measurements of D^{*+} and D^0 decays give $BR(D^{*+} \rightarrow D^0\pi) = .64 \pm .11$ and $BR(D \rightarrow K\pi) = .026 \pm .06$ (61). After background subtraction there are 42 ± 8 $\mu^+\mu^-$ events between 2.7 and 3.2 GeV/c^2 in Fig. 19(a). With this information, and the acceptances and efficiencies for D* and J/ψ events given previously, the 82 ± 25 D* events (Table 6) give $d\sigma/dx\big|_{x=.03} = 7 \pm 3$(statistical) ± 3(systematic) $\mu b/$(unit x) or $d\sigma/dy\big|_{y=0} = \{2M_{D^*}/\sqrt{s}\}\, d\sigma/dx = 1.4 \pm .6$(statistical) $\pm .6$(systematic) $\mu b/$(unit y). If a $(1-|x|)^3 \exp\{-1.1p_T^2\}$ parameterization is assumed for the differential cross section, along with exact SU(3) symmetry that implies $D^{*+}/$(all D's) = 3/8, a total cross section for D production of 11 ± 4 μb is obtained.

As a check of the flux normalization, using the target thickness (1.2 cm.), the $\Delta x \langle A(\psi)\rangle$ calculated previously, and the π^- flux as measured by the ion chamber at the target and corrected for system deadtime ($.92\ 10^{13}\pi$), the 42 ± 8 $\mu^+\mu^-$ events with $2.7 < M_{\mu\mu} < 3.2$ GeV/c^2 give $d\sigma/dx\big|_{x=.07} = 13 \pm 3.6$ nb-(unit x)$^{-1}$ for $\pi^- N \rightarrow \mu^+\mu^-$. This is in good agreement with the $d\sigma/dx\big|_{x=.07} = 16 \pm 3$ nb-(unit x)$^{-1}$ obtained from Reference (62), with a 12% reduction for the lower energy of this experiment.

These results are in best accord with those from the prompt muon beam dump experiment at Fermilab and from the μ-e pair experiment run at the ISR. Larger cross sections are inferred from the prompt neutrino experiment at CERN, in the 25-50 μb range, the same range of cross sections that the groups looking for charm decay in optical detectors have reported. The final results presented in this report cannot be considered incompatible with these earlier cross section measurements because of the many assumptions that have been made in all cases. The hadronic charmed meson production rate reported here does appear sufficient to confirm that the decay of these short-lived particles is the major component of the signal seen in data from many detectors constructed to observe charm phenomena indirectly.

Appendix A

PARTICLE IDENTIFICATION

The two Cerenkov counters in a fast arm, both operating in a threshold mode, allowed definite identification of pions throughout the 4-70 GeV/c momentum acceptance of the arm. Kaons were separated from protons at momenta greater than 11 GeV/c. As mentioned before, all particles in the slow pion arm were assumed to be pions.

The CO_2 filled threshold counters were the primary means of identifying pions. Fig. 24((a) shows a sample pulse height spectrum from one of these counters for pions with $9.5 < P < 10.5$ GeV/c. Using a pulse height vs. momentum scatterplot, at a given momentum slice a threshold edge with 95% of the pions in the peak lying above that edge may be determined. The pion identification cut on threshold counter pulse height lies comfortably below the threshold edge, as shown in Fig. 24(b), except at lowest momenta. Below 7 GeV/c an additional requirement of a minimum pulse height in the sum of the two differential counter P.M. tubes was utilized for pion identification. In comparisons of the threshold and differential counter outputs the threshold counter was found to be $96 \pm 4\%$ efficient in pion identification.

Figure 24

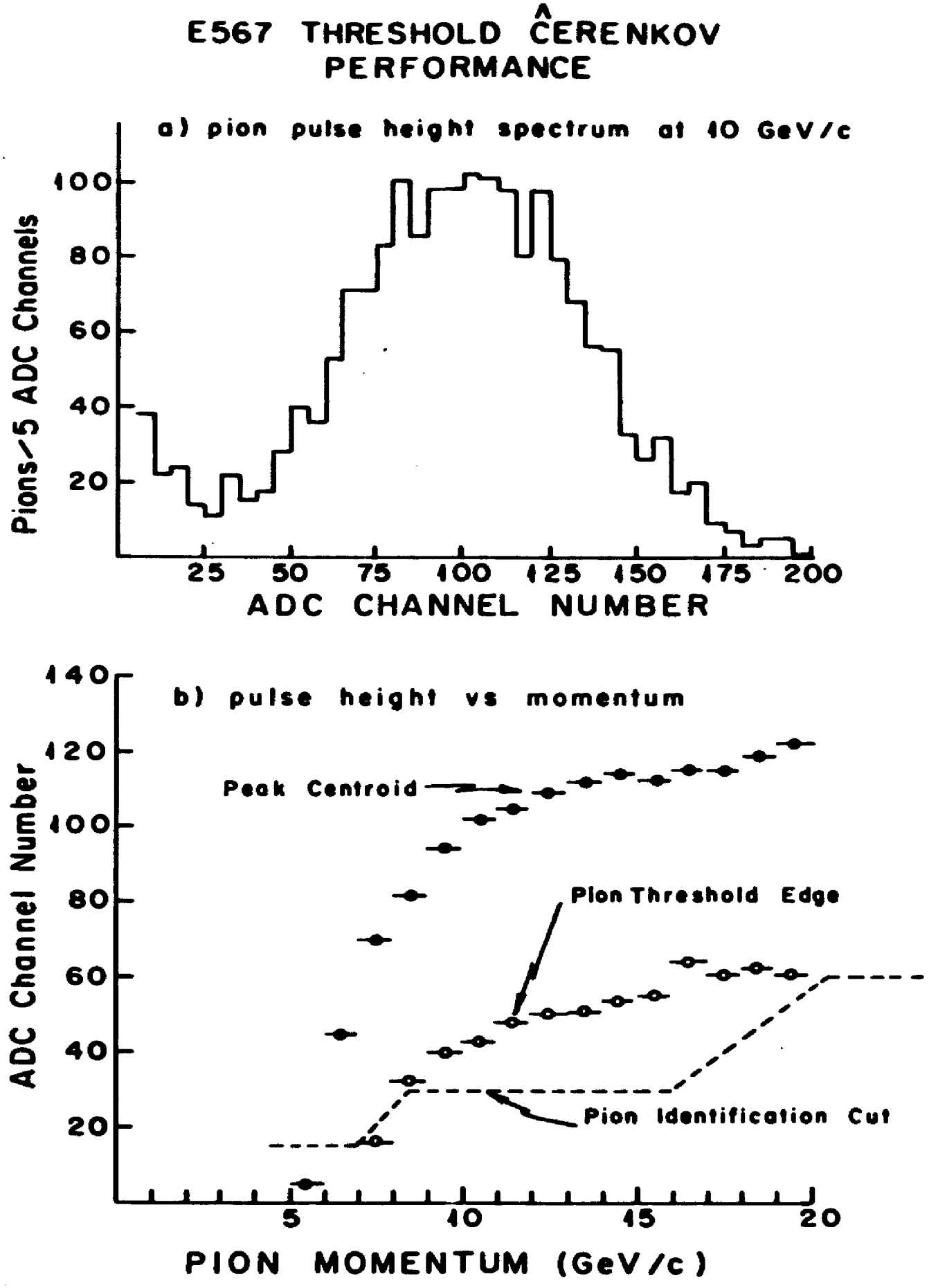
E567 THRESHOLD ČERENKOV PERFORMANCE
a) pion pulse height spectrum at 10 GeV/c
Pions/5 ADC Channels
100
80
60
40
20
25
50
75
100
125
150
175
200
ADC CHANNEL NUMBER
b) pulse height vs momentum
ADC Channel Number
140
120
100
80
60
40
20
Peak Centroid
Pion Threshold Edge
Pion Identification Cut
5
10
15
20
PION MOMENTUM (GeV/c)

Particles not meeting pion selection criteria were assumed to be kaons for P < 11 GeV/c. The differential counter had a threshold of 11 GeV/c for kaons, and the total pulse height sum of the inner and outer portions of the rosette mask could be used to tag kaons above Cerenkov threshold. The absence of any ϕ peak in Fig. 18(b) indicates the effectiveness of this identification scheme.

Muons were identified by their ability to penetrate the steel filters at the back end of the fast spectrometer arms. A significant fraction of hadrons were transmitted through the first filter segment, so only muon events registering in all three hodoscopes behind the steel filters were accepted as muons for the di-muon mass spectra in Fig. 19. The muon trigger logic had required that any two of these three hodoscopes detect a charged particle.

Appendix F

MASS RESOLUTION

The resolution for determining a particle's mass in a two body decay into the two fast spectrometer arms was limited by the relatively shortness of those arms. The intrinsic resolution of the drift chamber system in those two arms was determined to be .028" from the fitting residuals of the highest momentum tracks. Errors induced by multiple Coulomb scattering from the material in the arm were studied by plotting the deviations in chamber 3X as a function of momentum and agreed with estimates made using $\Delta\theta = 15\text{MeV}/P\sqrt{x/x^0}$, with the radiation lengths x^0 as tabulated in the Particle Data Book for the materials in the spectrometer arm. Monte Carlo simulation of tracks with multiple scattering, a chamber resolution of .032", and chamber hits randomly lost according to the statistics from the track finding program gave track fit statistics approximating those seen in primary analysis of the data. The 1.8% momentum resolution that is obtained from the Monte Carlo gives half widths in mass peaks of 14.4 and 38 MeV at the D mass and the J/ψ mass respectively. The observed J/ψ peak in Fig. 19(a) is consistent with this.

A major limitation to the three body mass resolution was the lack of track information for slow pions before the magnet in the third arm. The uncertainty in the decay vertex position, which was determined by the vertex obtained from the two fast arm tracks, was estimated to be .06" using the resolution Monte Carlo results. There was a systematic uncertainty in the bending plane center of the third spectrometer magnet. With these uncertainties, along with multiple scattering and a drift chamber system accuracy of .014", a 1% momentum resolution is achieved in the third arm. This leads to an Q-value resolution of .6 MeV/c for the apparatus.

When generating the Kπ mass spectra with the requirement that the three body Q-value be consistent with a D* parent it was decided to calculate an expected resolution in that variable based on each event's kinematics. This cut allowed us to optimize the signal to background in the mass spectra.

From the definition of Q-value Q = EM3 - EM2 - M_π, where EM3 is the D* invariant mass from the three body data and EM2 is the D mass calculated from the K-π momenta, an error for each event can be assigned. Since

$$\Delta Q = \sqrt{\left(\frac{\partial Q}{\partial P_K}\frac{\partial P_K}{\partial \theta_{DJ}} + \frac{\partial Q}{\partial \theta_{D\pi}}\frac{\partial \theta_{D\pi}}{\partial \theta_{DJ}}\right)\Delta\theta_{DJ}^2 + \left(\frac{\partial Q}{\partial \theta_{D\pi}}\frac{\partial \theta_{D\pi}}{\partial \theta_{DK}}\right)^2\Delta\theta_{DK}^2 + \left(\frac{\partial Q}{\partial P_\pi}\right)^2\Delta P_\pi^2 + \left(\frac{\partial Q}{\partial \theta_{D\pi}}\frac{\partial \theta_{D\pi}}{\partial \theta_{DJ}}\right)^2\Delta\theta_{MS}^2}$$

$$\frac{\partial Q}{\partial P_K} \cong 1/EM3\,(E_D \cdot P_\pi / E_\pi - P_D \cos\theta_{D\pi}) \qquad \frac{\partial Q}{\partial \theta_{D\pi}} = 1/EM3\,(P_D\, P_\pi \sin\theta_{D\pi})$$

$$EM3 = \sqrt{(E_D + E_\pi)^2 - (P_D + P_\pi)^2}$$

separating the sources of error in the slow pion 4-momentum determination. These errors were determined to be:

$\Delta\theta_{ms}/P_\pi$ = .0025 multiple scattering in the target
$\Delta P_\pi/P_\pi$ = .004 verter and H.B. field determination
$\Delta\theta_2$ = .0022 slow arm non-bending plane angle determination
$\Delta\theta_3$ = .0016 slow arm bending plane angle determination

Defining a quantity $\delta Q = (Q \text{ measured} - 5.9)/\Delta Q$ for each event gave a consistent way to apply the Q-value information in making cuts on the K_π mass data.

For a Gaussian peak with half-width σ superimposed on a linear background with Poisson fluctuations it is easy to show that the optimum peak to background ratio is acheived by restricting the data sample to within $|1.3\ \sigma|$ of the peak value.

REFERENCES

1. M. Gell-Mann, Phys. Lett. , 8, (1964), 214.

2. D. Politzer, Phys. Rev. Lett. 30, (1973), 1346. D. Gross and F. Wilczek, Phys. Rev. Lett. 30, (1973), 1343.

3. O.W. Greenberg, Phys. Rev. Lett. 13, (1964), 598.

4. S. Glashow et al. ,Phys. Rev. D2,(1970),1285.

5. P. Tarjanne and V. Teplitz, Phys. Rev. Lett., 11, (1963), 447.

6. B. J. Bjørken and S. L. Glashow, Phys. Lett., 11, (1964), 255.

7. D. Amati et al., Phys. Lett., 11, (1964), 190.

8. J. Bernstein, Elementary Particles and their Currents, W. H. Freeman & Co., New York, (1968), 191.

9. M. Shochet et. al.,Phys. Rev. D19, (1979), 1965.

10. Z. Maki, Prog. in Theo. Phys., 31, (1964), 331.

11. J.A. Augustin et al, Phys. Rev. Lett., 33, (1974), 1406.

12. J. Aubert et al., Phys. Rev. Lett., 33, (1974), 1404.

13. A. Benvenuti et al., Phys. Rev. Lett. 34, (1975), 419.
B.C. Barish et al., Phys. Rev. Lett. 36, (1976), 939.
M. Holder et al., Phys. Lett. 69B, (1977)
C. Baltay et al., Phys. Rev. Lett. 39, (1977), 62.

14. C. Baltay, XIX International Conference on High Energy Physics, Tokyo, (1978).

15. M. Gaillard,B. Lee, J. Rosner, Rev. of Mod. Phys., 47, (1975), 277.

16. G.J. Feldman et al., Phys. Rev. Lett., 38 , (1977), 1313.
G. Goldhaber et al., Phys. Rev. Lett., 37, 255, (1976).
I. Peruzzi et al., Phys. Rev. Lett., 37 , (1976), 569.

17. C. Baltay et al., Phys. Rev. Lett. 41, (1978), 73.

18. E. Cazzoli et al., Phys. Rev. Lett., 34, (1975), 1125.

19. D. Drijard et al. Phys. Lett.,85B, (1979), 452.
K. Giboni et al., Phys. Lett., 85B, (1979), 437.
W. Lockman et al., Phys. Lett., 85B, 1979), 443.

20. G. S. Abrahams et al., SLAC Preprint Pub-2406, (1979).

21. R. Brandelik et al., Phys. Lett., 80B, (1979), 412. F. Richard, Proceedings of International Symposium on Lepton and Photon Interactions 1979, Editors T. Kirk and H. Abarbanel, p469.

22. N. Ushida et al., "Measurement of D^+, F^+, and Λ_C Charmed Particle Lifetimes", Preprint DOE /ER/0154-278, (1980).
R. Ammar et al., Preprint submitted to Phys. Lett. B, (1980).

23. S. Herb et al., Phys. Rev. Lett., 39, (1977), 252.

24. W. Bartel et al., Phys. Lett. 89B, (1979), 136. D. P. Barber et al., Phys. Lett. 85B, (1979), 463. Ch. Berger et al., Phys. Lett. 86B, (1979), 413. R. Brandelik et al., DESY Preprint 79/74, (1979).

25. V. Luth, Proceedings of International Symposium on Lepton and Photon Interactions 1979, Editors T. Kirk and H. Abarbanel, p78.

26. H. Georgi et al., Annals of Phys., 114, (1978), 273.

27. B. Ioffe, Phys. Rev. Lett., 39, (1977), 1599.

28. G. E. Hogan et al., Phys. Rev. Lett., 43, (1979), 948.
C. Kourkoumelis et al., Phys. Lett., 91B, (1980), 481.

29. J.H. Cobb et al. Phys. Lett., 72B, (1978), 497.

30. A. Buras and K. Gaemers, Nucl. Phys., B132, (1978), 249.

31. M. Gluck, J. Owens, E. Reya, Phys. Rev., D17, (1978), 2324.

32. M. Gluck and E. Reya, Nucl. Phys., B130, (1976), 1922.

33. C.E. Carlson and R. Suaya, Phys. Lett., 81B, (1979), 329.

34. S. J. Brodsky et al., Nordita Preprint 80/18, (1980).

35. J. Mueller, Ph. D. Thesis, Princeton University, (1980), (unpublished).

36. F. Busser et al., Nucl. Phys., B113, (1976), 189.

37. M. Bourquin and J. M. Gaillard, Nucl. Phys., B141, (1976), 334.

38. M. Holder et al., Nucl. Inst. and Meth., 148, (1978), 235.

39. A. Diddens et al., "A Detector for Neutral-Current Interactions of High Energy Neutrinos", CERN Preprint EP80-63 submitted to Nucl. Inst. & Meth., (1980).

40. H. Wachsmuth, CERN Preprint EP79-115, (1979).

41. A. Bodek, Invited Talk at APS Div. of Particles and Fields Meeting, Montreal Canada, (1979).

42. M.S. Witherell, Invited Talk at XX Experimental Meson Spectroscopy Conference, Brookhaven, N.Y., (1980).

43. A. Chilingarov et al., Phys. Lett., 83B, (1979), 136.

44. T. Gaisser and F. Halzen, Phys. Rev., D14, (1976), 3153.

45. H. Fuchi et al., Phys. Lett., 85B, (1979), 135.

46. J. Sandweiss et al., Phys. Rev. Lett., 44, (1980), 1104.

47. W. Allison et al., CERN Preprint EP-49, (1980).

48. D. Drijard et al., Phys. Lett., 81B, (1979), 250.

49. J. Kirkby, Proceedings of International Symposium on Lepton and Photon Interactions 1979, Editors T. Kirk and H. Abarbanel, p107.

50. W. Ditzler et al., Phys. Lett., 71B, (1977), 451.

51. R. Cester et al., Phys. Rev. Lett., 42, (1978), 139.

52. P. Avery et al., Phys. Rev. Lett., 44, (1980), 1309.

53. V. L. Fitch, A Broad-Band Focusing Cerenkov Counter, (unpublished) Princeton University Technical Report.

54. B. Jean-Marie et al., Nucl. Instr. & Meth., 159, (1979), 213.

55. R. Cester-Regge et al., IEEE Trans. on Nucl. Sci.,25, (1978), 53.

56. P. Perez, Thesis'Etude de Grandes Chambres a Derive de Haute Precision', University of Paris-South, Orsay Pub. 2393, (1978).

57. M. Banner et al., Phys. Lett., 41B, (1972), 547.

58. M. Bourquin and J. M. Gaillard, op. cit..

59. K. J. Anderson et al., Phys. Rev. Lett. 42, (1979), 944.

60. J. G. Branson et al., Phys. Rev. Lett. 38, (1977), 1331.

61. J. Kirkby, op. cit..

62. G. E. Hogan, Ph. D. Thesis, Princeton University, (1979), (unpublished).